Discrete Fiber Raman Amplifiers with Incoherent Pumping

Jing Hong Fan

A Thesis

In

The Department

Of

Electrical and Computer Engineering

Presented in Partial Fulfillment of the Requirements
for the Degree of Master of Applied Science(Electrical Engineering) at
Concordia University
Montreal, Quebec, Canada

January 2005

Your file Votre référence
ISBN: 0-494-04367-9
Our file Notre référence
ISBN: 0-494-04367-9

ABSTRACT

Discrete Fiber Raman Amplifiers with Incoherent Pumping

Jing Hong Fan

In this thesis, C-band, L-band, and C+L-band DisFRAs with incoherent pumping are investigated respectively considering gain, NF, NF ripple, OSNR, OSNR ripple, and pumping efficiency with comparison to coherent pumping. All comparisons are based on the same average gain.

Increasing the spectral bandwidth of incoherent pumping source will result in reduction of gain ripple, NF ripple, and OSNR ripple exponentially in dB and accordingly increase of pumping power exponentially in mW. The average NF and OSNR keep almost unchanged with the increase of FWHM of incoherent pumping source. To achieve the same gain flatness the number of pumps for DisFRAs with incoherent pumping can be significantly reduced compared to coherent pumping.

The comparisons of C-band, L-band, and C+L-band DisFRAs with incoherent co-pumping to incoherent counter-pumping show that DisFRAs with incoherent co-pumping perform better because of flatter NF and OSNR, lower NF, higher OSNR, and increased pumping efficiency.

ACKNOWLEDGMENTS

Most of all, I would like to express my great gratitude to my research advisor Professor John X Zhang for his support and guidance over the past two years. His high expectation and enlightening advices have helped me stay improved, and made this thesis possible. I also should give my great thanks to Idan Mandelbaum, the author of "Raman amplifier model in single-mode optical fiber", IEEE Photon. Tech. Lett., vol.15, pp. 1704-1706 , 2003, for his help in verification of DisFRA model, and P. Gaarde, OFS Denmark, for providing the fiber parameters.

I would like to thank Natural Science of Engineering Research Council of Canada and Faulty of Electrical and Computer Science Engineering at Concordia University to support this project.

Learning together with other members in fiber optic communication system field has greatly enriched my education and life. I would like to thank all of them for their support and encouragement: Ting Zhang, Bin Han, Lei Wang, and Yong Mei Zhu. Their suggestions made the task of research enjoyable.

Finally, but not at least, I would like to thank my husband, my parents, and my four-month daughter, their love and encouragement made me overcome difficulties and complete this degree.

TABLE OF CONTENTS

LIST OF FIGURES

LIST OF TABLES

CHAPTER 1 INTRODUCTION

This chapter first briefly describes the evolution of optical fiber communication in Section 1.1. The description is followed by a discussion on the types of optical amplifiers in Section 1.2. Background, motivation and simulation results in this thesis are briefly presented in Section 1.3. Our main focus is on the performance improvements, which are produced by using incoherent pumping instead of coherent pumping. The structure of the thesis is described in Section 1.4 - for each chapter the main contents are described.

1.1 Evolution of optical fiber communication

The first optical fiber [1] exhibited high attenuations of 1000 dB/km and was actually a lot worse than available coaxial cables, which had attenuations of 5-10 dB/km [2]. This changed a lot in the next decades, and a break-through occurred when the fiber attenuation was reduced to 20 dB/km [3] in 1970 and to 0.2 dB/km (in the 1550 nm region) in 1979 [4].

The first generation of optical fibers used multi-mode fiber in the first telecommunication window around 0.8 μm. A bit-rate distance product of ~500 Mb/s • km was achieved with this generation.

The second generation of optical fibers utilized the second telecommunication window around 1.3 μm, where the fiber has lower loss. Some multi-mode fibers were

replaced with single-mode fiber. This generation could provide a bit-rate distance product of > 100 Gb/ s • km.

The third generation of optical fibers exploited the minima in fiber loss, which is in the third telecommunication window, i.e. 1.55 μm. This generation could achieve a bit-rate distance product of >1000 Gb/ s • km.

The introduction of optical amplifiers revolutionized the field of optical fiber communications. The newest generation of optical fiber communication systems uses wavelength division multiplexing (WDM) to increase system capacity, resulting in capacity distance product of $>1{,}400$ Tb/s • km.

1.2 Optical amplifiers

This section presents the basics of optical amplifiers and classifies the three fundamental amplifier types: semiconductor optical amplifiers (SOAs), erbium-doped fiber amplifiers (EDFAs), and fiber Raman amplifiers (FRAs).

The first really useful type of optical amplifiers was SOA [1]. The SOAs had many properties common with single longitudinal mode lasers: They were just lasers with anti-reflection coating on each facet to remove the feedback. Nowadays SOAs are mostly used as wavelength converters, optical clock and data regenerators.

The EDFA, which is made of a silica fiber doped with erbium, was first presented in 1986 [5-7]. Used as inline amplifiers the EDFA has made possible virtually unlimited transmission distance when used together with a transmission format that either utilizes

or compensated for the accumulated dispersion and nonlinearities. The operation of an EDFA by itself normally is limited to from 1530 to 1560 nm region.

The main advantage of the FRAs over any other types of optical amplifiers is its ability to be used in any wavelength region [8][9], because the spectrum is only decided by the pump wavelength. Broadly speaking, there are two classes of Raman amplifiers [8]. One is distributed fiber Raman amplifiers (DFRAs), so called because the gain is distributed along the transmission fibers. The other is discrete fiber Raman amplifiers (DisFRAs) because the gain occurs within discrete elements in transmission systems. FRAs are quite suitable for high-capacity dense wavelength division multiplexing (DWDM) transmission systems [10] due to improved optical signal to noise ratio (OSNR) and reduced fiber nonlinear impairments [11].

FRAs provide wide-band (~100-nm) amplification of optical signals in high-capacity DWDM transmission systems using multiple high-power pumps of different wavelengths. The gain profile can be flattened by appropriately choosing the relative wavelengths and powers of the pump waves [12]. One of the challenges for FRAs application in DWDM is to combat the pumping induced impairments, such as four-wave-mixing (FWM) and Stimulated Brillouin scattering (SBS). The FWM can be generated by the interaction of pump-to-pump, pump-to-amplified spontaneous emission (ASE), and pump-to-signals; and the SBS can be resulted from each of high-power pumping sources [13][14]. Time-division multiplexed (TDM) pumping [15-17], where different pump wavelengths are temporarily separated, is used to overcome the FWM impairment. The drawbacks of

TDM are increased double Rayleigh scattering [15] and ASE noise [16]. A spool of high-dispersion fiber inserted at pump output [16] was proposed to suppress the FWM impairment, but resulting in additional loss [18].

1.3 Motivations of this thesis

The study presented in this thesis was inspired by the successful use of high-power (>450 mw) incoherent semiconductor pumping sources [19]. The ability to create modules with more than 450 mw of broadband pump light allows us to address many of these FRA limitations in a fundamental manner.

The flatness of gain spectrum, which is measured by the gain ripple, is a critical challenge in FRAs design and is especially important for long-haul transmission systems since the difference in gain of each span will be accumulated at output. With the increase of pump numbers, the gain flatness is improved, but the FRAs design becomes more complicated and time consuming [12]. In the past, only the coherent pumping sources, in which the power is located within a narrow bandwidth around the pump central-frequency, were employed. Raman gain is polarization sensitive [20]. Traditionally, to reduce the polarization dependent gain, each coherent pump wavelength requires light to be launched at two orthogonal linear polarizations, which is complicated and costly. The motivation of this thesis is to optimize the FRAs design and reduce the complication and the cost.

In contrast to the conventional coherent pumping source, the pumping power of incoherent pumping source spreads over a wide wavelength ranged from several nanometers to tens of nanometers, and the phase and polarization of incoherent pumping source are completely random. The performance of DisFRAs with incoherent pumping is investigated in the thesis. The results show that the incoherent pumping has several advantages. Firstly, to obtain the same gain flatness, the number of pumps required by using incoherent pumping is significantly reduced compared to coherent pumping. Secondly, incoherent pumping inherently eliminates the polarization multiplier due to the random polarization of incoherent pumping sources [19]. As a result, the DisFRAs with incoherent pumping become less complicated and cost effective. Thirdly, the SBS impairment can be completely overcome by using incoherent pumping due to its wide spectral width. Fourthly, the FWM generation by the interaction of pump-pump, pump-ASE noise and pump-signal can be significantly reduced due to the random phase of incoherent pumping sources.

Increasing the spectral bandwidth of incoherent pumping source will result in reduction of gain ripple, noise figure (NF) ripple, and OSNR ripple exponentially in dB and increase of pumping power exponentially in mW. The average NF and OSNR keep almost unchanged with the increase of FWHM of incoherent pumping source. To achieve the same gain flatness the number of pumps for DisFRAs with incoherent pumping can be significantly reduced compared to coherent pumping. The comparisons of C-band, L-band, and C+L-band DisFRAs with incoherent co-pumping to incoherent

counter-pumping show that DisFRAs with incoherent co-pumping perform better because of flatter NF and OSNR, lower NF, higher OSNR, and increased pumping efficiency. The performance of DisFRAs with coherent co-pumping is also superior to coherent counter-pumping due to flatter NF and OSNR, lower NF, higher OSNR, and increased pumping efficiency.

1.4 Thesis structure

The structure of the thesis is described in this section – for each chapter the main contents are described.

In Chapter 2, the theory of the fiber Raman amplification process is described. First a basic description of Raman scattering is presented in Section 2.1. Then, the principles of FRAs as well as basic definitions of gain, NF, and OSNR are given in Section 2.2.

In Chapter 3, a general continuous wave (CW) FRA model is presented in Section 3.1. It takes all effects considered to be of interest in practical FRAs into account: attenuation, pump-to-pump, signal-to-signal, pump-to-signal interactions, Rayleigh scattering, multiple-path interference (MPI), Stokes, and anti-Stoke spontaneous emissions. The description of a new method of gain scaling is followed in Section 3.2.

In Chapter 4, the mechanism of high-power incoherent pumps is presented in Section 4.1. This was achieved through coupling of a low-power seed optical signal from a semiconductor ASE source into a long-cavity semiconductor amplifier waveguide, which was optimized in design for CW power amplification. The numerical model for

incoherent pumping is introduced in Section 4.2.

In Chapter 5, C-band DisFRAs with counter-pumping are analyzed in Section 5.1 and with co-pumping are analyzed in Section 5.2. In these two sections, we separately explore the relationship of gain ripple, average NF, NF ripple, average OSNR, OSNR ripple and pumping efficiency with FWHM of an incoherent pumping source and compare the performance of C-band DisFRAs with multiple incoherent pumping sources to multiple coherent pumping sources. The performance of C-band DisFRAs with incoherent co-pumping is compared to incoherent counter-pumping in Section 5.3. The simulation results show that C-band DisFRAs with incoherent co-pumping are superior to incoherent counter-pumping due to flatter NF and OSNR, lower NF, higher OSNR and increased pumping efficiency.

In Chapter 6, L-band DisFRAs with counter-pumping are analyzed in Section 6.1. Our investigation explores the relationship of gain ripple, average NF, NF ripple, average OSNR, OSNR ripple, and pumping efficiency with FWHM of an incoherent counter-pumping source and compares the performance of L-band DisFRAs with multiple coherent counter-pumping sources to multiple incoherent counter-pumping sources. The above investigation is also carried out in Section 6.2, however, L-band DisFRAs are co-pumped. The performance of L-band DisFRAs with incoherent co-pumping is compared to incoherent counter-pumping in Section 6.3. Simulation results show that L-band DisFRAs with incoherent co-pumping are preferred due to flatter NF and OSNR, lower NF, higher OSNR, and increased pumping efficiency.

In Chapter 7, We compare the C+L-band DisFRAs with two incoherent counter-pumping sources to two, or four, or six coherent counter-pumping sources in terms of gain ripple, average NF, NF ripple, average OSNR, OSNR ripple and pumping efficiency in Section 7.1. We also compare the performance of C+L-band DisFRAs with two incoherent co-pumping sources to multiple coherent co-pumping sources in Section 7.2. The performance of C+L-band DisFRAs with incoherent co-pumping is compared to incoherent counter-pumping in Section 7.3. Simulation results show that C+L-band DisFRAs with incoherent co-pumping perform better because of flatter NF and OSNR, lower NF, higher OSNR, and increased pumping efficiency.

In Chapter 8, concluded this thesis and summarized all the results shown in all the previous chapters.

CHAPTER 2 FIBER RAMAN AMPLIFIER THEORY

This chapter presents the theory of the fiber Raman amplification. First a basic description of Raman scattering is presented in Section 2.1. Then, the principle of FRAs as well as basic definitions of gain, NF, and OSNR is given in Section2.2.

2.1 Raman scattering

Spontaneous Raman scattering was first discovered by Raman, for which he received the Nobel Prize in Physics in 1930 [21]. The energy diagram shown in Figure 2.1 can describe Raman scattering. There are basically two types of Raman scattering process [1]:

- Absorption of a pump photon followed by a change in vibrational energy of the participation molecule and the emission of a photon with the energy difference. This is called Stokes scattering.

- If the pump photon is absorbed by a molecule that is already excited, a photon with energy equal to the sum of energies is emitted. This is called anti-Stokes scattering. It only takes place for a fiber temperature above the absolute zero – non-zero population of the excited vibrational state is needed,

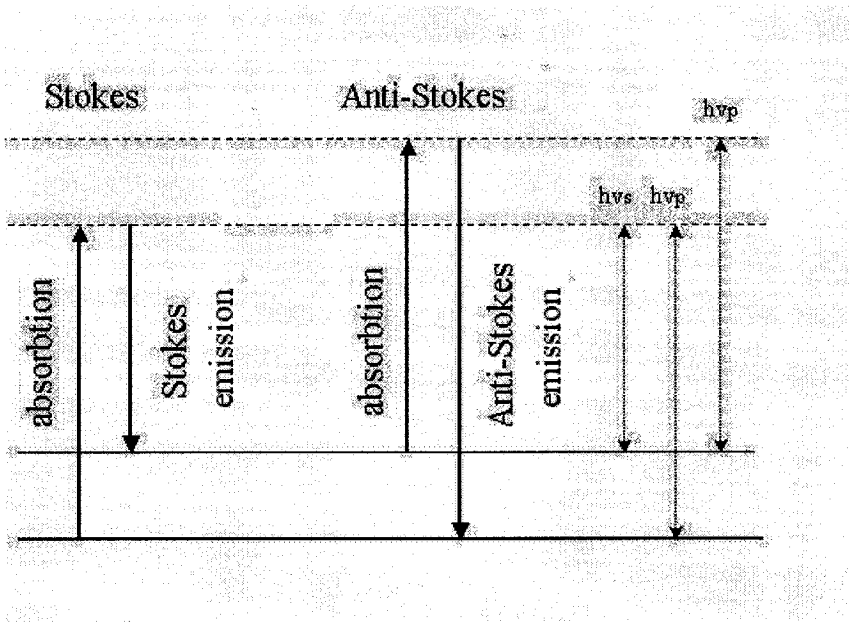

Figure 2.1 - Energy diagram for the Raman scattering processes: Stokes scattering and anti-Stoke scattering

The Raman scattering process becomes stimulated if the pump power exceeds a threshold value [10]. Stimulated Raman Scattering (SRS) can occur in both the forward and the backward directions in optical fibers.

2.2 Raman amplification

Raman amplification is becoming increasingly important in optical communication systems as a tool for offsetting intrinsic fiber losses [22]. In a quantum mechanical description, shown in the energy-level diagram in Figure 2.2, a pump photon is converted into a second signal photon that is an exact replica of the first, and the remaining energy produces an optical phonon. The initial signal photon, therefore, has been amplified.

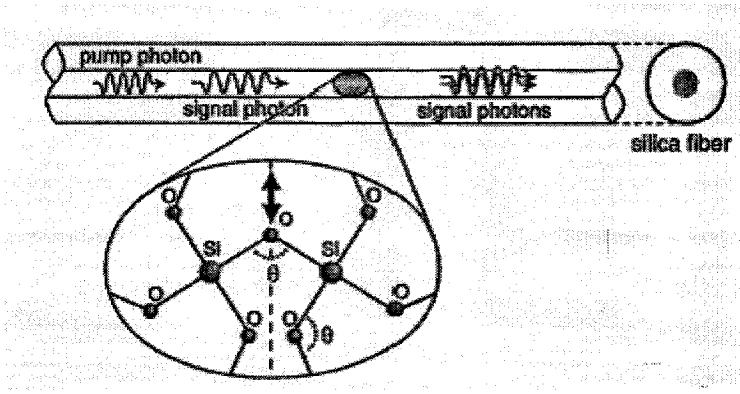

Figure 2.2 - Schematic depicting amplification by SRS in an optical silica fiber. The silica molecules convert the pump into a replica of the signal photon, producing an optical phonon

These Raman scattering processes can be used to provide amplification if signal photons having photon energies within the Raman line are injected together with a strong co-polarized pump [1]. No Raman amplification takes place if the signal and pump are launched in orthogonal polarizations. For unpolarized pumps the Raman gain is reduced by a factor of two.

The Raman gain coefficient is a fundamental parameter for Raman amplification. This parameter determines the strength of the coupling between a pump beam and a signal beam due to SRS [22]. The Raman–gain coefficient g_R is related to the optical gain $g(z)$ as g = $g_R I_p(z)$, where I_p is the pump intensity. In terms of the pump power P_p, the gain can be written as

$$g(\omega) = g_R(\omega)(P_p / a_p) \tag{2.1}$$

Here, a_p is the cross-sectional area of the pump beam inside a fiber. Since a_p can vary considerably for different types of fibers, the ratio g_R/a_p is a measure of the Raman-gain efficiency. This ratio is plotted in Figure 2.4 for three different fibers: a standard silica fiber (SMF), a dispersion-compensating fiber (DCF), and a TrueWave-Reach fiber, which are used in this thesis

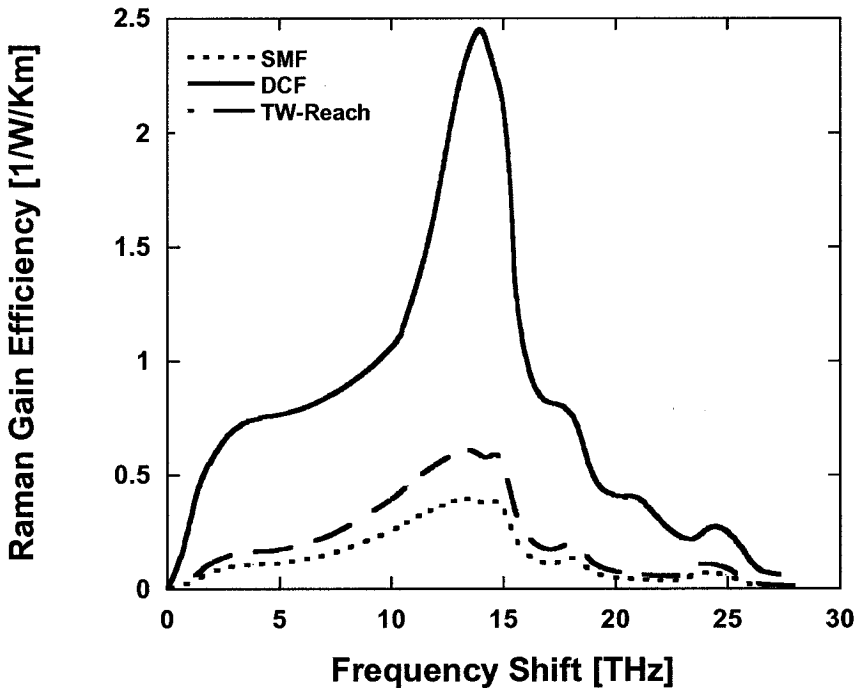

Figure 2.3 - Raman-gain spectra (ratio g_R / a_p) for SMF, DCF, and TW-Reach fibers

2.2.1 Raman gain

A. Properties of Raman gain from SRS

The following fundamental properties of SRS are critical for designing fiber Raman

amplifiers [8]:

1) Raman gain has a spectral shape that depends primarily on the frequency separation between a pump and signal, not their absolute frequencies. This follows from energy conservation: their frequency separation must equal the frequency of the optical phonon that is created.
2) Raman gain is polarization dependent. The peak coupling strength between a pump and signal is approximately an order of magnitude stronger if they are co-polarized than if they are orthogonal polarized.
3) Raman gain does not depend on the relative direction of propagation of a pump and signal.

B. Amplification of a signal by a pump

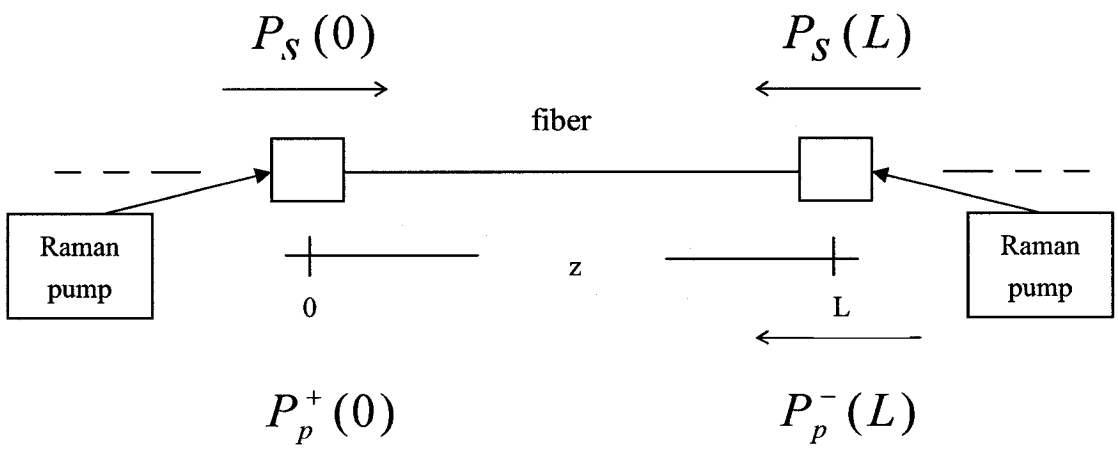

Figure 2.4 - Schematic of a simple Raman fiber amplifier, which is both co-pumped and counter-pumped

Figure 2.4 shows a schematic of a simple Raman amplifier. It consists of a length of L fiber that is both co pumped and counter pumped with pump powers P_p^+ and P_p^-, respectively [8]. (Throughout this thesis, it is assumed that the signal propagates in the +z -direction). The Raman gain of the FRA is given by

$$G = \frac{P_s(L)}{P_s(0)} \tag{2.2}$$

2.2.2 Noise figure

A. Sources of noise

In addition to producing gain, Raman amplification also produces noise. Understanding how much is produced is crucial because noise accumulation causes transmitted information to be corrupted [8].

The most important source of noise is ASE, which is an unavoidable by-product of gain in all-optical amplifiers. In the case of FRAs, spontaneous Raman scattering generates ASE. ASE generation is important because it leads to noise. The dominant type of noise occurs when signal light interferes with co-polarized ASE that is propagating in the same direction, producing intensity fluctuations called "signal-spontaneous beat noise." The temperature dependence of the emission spectrum is described by multiplying the gain spectrum with a correction factor, which is called the excess spontaneous emission noise (XSE). This excess spontaneous emission noise n^{XSE} is

defined by [1]:

$$n^{XSE}(v_i - v_j, T) = \begin{cases} \frac{1}{e^{h(v_i - v_j)/KT} - 1} & for \quad v_i - v_j < 0 \\ 1 + \frac{1}{e^{h(v_i - v_j)/KT} - 1} & for \quad v_i - v_j > 0 \end{cases} \tag{2.3}$$

Where h and k is Planck's and Boltzmann's constants, respectively. $v_i - v_j$ is the frequency difference between signal and pump and T is the absolute temperature. The excess noise at the Raman gain peak is 0.5 dB at room temperature (300K). For wavelengths closer to the pump, much more excess noise is produced. When the absolute temperature approaches zero, n^{XSE} becomes one, which is the value used in all recent Raman modeling [1].

Noise from multiple-path interference (MPI) occurs when signal light reaches the receiver by more than one optical path [8]. The simplest example occurs when there are two reflection sites along a system. A small portion of the signal light can be delayed as it is multiply reflected between these sites. Therefore, there are two types of light present at the receiver: the "straight-through" light with average power P_s, and delayed light with power P_{MPI}. MPI results in double-Rayleigh backscattering (DRB), when the signal is backscattered twice. DRB limits gain in DisFRAs, which typically use several kilometers of fiber to make efficient use of the pump light [23]. For the DisFRAs, the noise degradation increases rapidly with gain.

Single-pass reflections of backward traveling noise into the forward direction

manifest itself as an increase in NF, thereby making the amplifier noisier especially for DisFRAs with counter-pumping. Almost all the reflected noise has the larger gain at the amplifier output end compared to co-pumping.

B. Noise figure

An optical amplifier's NF quantifies how much the amplifier degrades signal-to-noise (SNR) of a signal when the signal is amplified [8][24]. It is defined as

$$\mathrm{NF} = \frac{(SNR)_{in}}{(SNR)_{out}} \tag{2.4}$$

When both ASE noise, which is an optical broadband source of white noise, and MPI, which is an optical narrowband source of colored (nonwhite) noise, are included, a complicated expression for calculating NF of an amplifier is given in [25]. However, it was shown by experiments that Equation (2.5), which is given in [24], still provides a very good approximation. Therefore Equation (2.5) is always used in calculating NF in this thesis.

$$\mathrm{NF} = \frac{1}{G}\left(1 + \frac{P^{+}_{ASE}(L) + P^{+}_{MPI}(L) + P^{+}_{reflected}(L)}{h\nu\Delta\nu}\right) \tag{2.5}$$

Where ν is the signal frequency, $\Delta\nu$ is the given reference bandwidth (1 nm in this thesis) around the signal frequency, and $P^{+}_{ASE}(L)$, $P^{+}_{MPI}(L)$, and $P^{+}_{reflected}(L)$ are the power of ASE, MPI, and Single-pass reflected noise at the boundary of $z = L$,

respectively. Unlike the Raman gain, the amplifier NF is temperature-dependent.

2.2.3 Optical signal-to-noise ratio

Several quantities can be used to describe the noise properties of Raman amplifiers. One is the OSNR. This is defined as the ratio of the optical signal power to the power of the noise in a given reference bandwidth around the signal wavelength.

$$\text{OSNR}=\frac{P_S^+(L)}{P_{noise}^+(L)} \tag{2.6}$$

In this thesis, signal spacing is different from noise spacing. The unit of signal spacing is GHz and the unit of noise spacing is 1 nm. As a result, the above equation can be written as

$$\text{OSNR}=\frac{P_S^+(L)}{P_{noise}^+(L)}\cdot\frac{\frac{C}{\lambda^2}\cdot\Delta\lambda}{\Delta\nu} \tag{2.7}$$

Where, λ is the wavelength of the signal, $\Delta\lambda$ is the noise spacing (1 nm), and $\Delta\nu$ is the signal spacing.

CHAPTER 3 MODELING OF FIBER RAMAN AMPLIFIERS

This chapter introduces a general FRA model in Section 3.1. It takes all effects considered to be of interest in practical FRAs into account: attenuation, pump-to-pump, signal-to-signal, pump-to-signal interactions, Rayleigh scattering, MPI, Stokes, and anti-Stoke spontaneous emissions. The verification of this model is followed. A new method for scaling the Raman gain coefficient is described in Section 3.2. How to scale the Raman gain coefficient from the measured at one pump wavelength to a new pump wavelength is demonstrated.

3.1 FRA model

The accurate modeling of Raman amplification is extremely important for modern communication system design [26]. This section describes the FRA model presented in the thesis. This model was constructed that simulates all of the physical properties that may affect the validity of the model. The following effects were included along with the capability of modeling any number of signals and pumps [27]:

- Attenuation
- Rayleigh scattering from the backward power (including ASE noise)
- Raman gain pumped by signals, bi-directional pumps/ASE noise, which have higher frequencies (or shorter wavelengths)
- Pump depletion by signals, bi-directional pumps, which have lower frequencies (or

higher wavelengths)

- ASE noise generated (or Stokes) by signals, bi-directional pumps/ASE noise, which have higher frequencies (or shorter wavelengths)
- ASE noise generation (Anti-Stokes emission) by signals, bi-directional pumps/ASE noise, which have lower frequency or higher wavelength

The distribution of pumps, signals, and ASE in an optical fiber is plotted in wavelength in Figure 3.1 (a) and in frequency in Figure 3.1 (b).

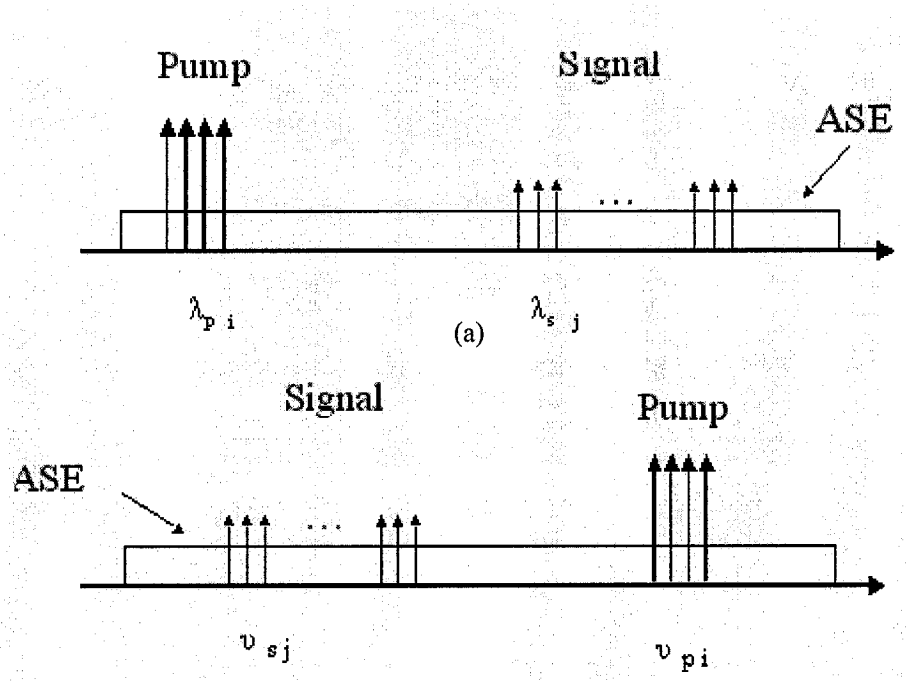

Figure 3.1 - Illustration of frequency intervals for the numerical calculation. The entire spectral range of interest is represented in (a) wavelength and (b) frequency

The liner and nonlinear effects couple signals/pumps propagating in the same and opposite directions, and to solve their propagation equations becomes a two-point boundary problem [28]. For the FRA systems, the iterative method is usually used to solve such a problem. The model numerically solves the Equation (3.1a) for the forward propagation wave simultaneously for all frequencies v [26] and Equation (3.1b) for the backward propagating wave. The forward propagation equation is given by

$$\begin{aligned}
\frac{dP_f(z,v_i)}{dz} &= -\alpha(v_i)P_f(z,v_i) \\
&\quad + \gamma(v_i)P_b(z,v_i) \\
&\quad + P_f(z,v_i)\sum_j^{v_j>v_i}\frac{g_R(v_j,v_i)}{A_{eff}(v_j,v_i)}\left[P_f(z,v_j)+P_b(z,v_j)\right] \\
&\quad + 2hv_i\Delta v\sum_j^{v_j>v_i}\frac{g_R(v_j,v_i)}{A_{eff}(v_j,v_i)}\left[P_f(z,v_j)+P_b(z,v_j)\right]\left(1+\frac{1}{e^{\frac{h(v_j-v_i)}{kT}}-1}\right) \\
&\quad - P_f(z,v_i)\sum_j^{v_j<v_i}\frac{v_j}{v_i}\frac{V_j}{V_i}\frac{g_R(v_i,v_j)}{A_{eff}(v_i,v_j)}\left[(P_f(z,v_j)+P_b(z,v_j)\right] \\
&\quad + 2hv_i\Delta v\sum_j^{v_j<v_i}\frac{v_j}{v_i}\frac{V_j}{V_i}\frac{g_R(v_i,v_j)}{A_{eff}(v_i,v_j)}\left[(P_f(z,v_j)+P_b(z,v_j)\right]\frac{1}{e^{\frac{h(v_i-v_j)}{kT}}-1}
\end{aligned} \tag{3.1a}$$

The backward propagation equation is given by

$$\frac{dP_b(z,\nu_i)}{dz} = -\alpha(\nu_i)P_b(z,\nu_i)$$

$$+\gamma(\nu_i)P_f(z,\nu_i)$$

$$+P_b(z,\nu_i)\sum_j^{\nu_j>\nu_i}\frac{g_R(\nu_j,\nu_i)}{A_{eff}(\nu_j,\nu_i)}\left([P_f(z,\nu_j)+P_b(z,\nu_j)\right]$$

$$+2h\nu_i\Delta\nu\sum_j^{\nu_j>\nu_i}\frac{g_R(\nu_j,\nu_i)}{A_{eff}(\nu_j,\nu_i)}\left[P_f(z,\nu_j)+P_b(z,\nu_j)\right]\left(1+\frac{1}{e^{\frac{h(\nu_j-\nu_i)}{kT}}-1}\right) \qquad (3.1b)$$

$$-P_b(z,\nu_i)\sum_j^{\nu_j<\nu_i}\frac{\nu_j}{\nu_i}\frac{V_j}{V_i}\frac{g_R(\nu_i,\nu_j)}{A_{eff}(\nu_i,\nu_j)}\left[(P_f(z,\nu_j)+P_b(z,\nu_j)\right]$$

$$+2h\nu_i\Delta\nu\sum_j^{\nu_j<\nu_i}\frac{\nu_j}{\nu_i}\frac{V_j}{V_i}\frac{g_R(\nu_i,\nu_j)}{A_{eff}(\nu_i,\nu_j)}\left[(P_f(z,\nu_j)+P_b(z,\nu_j)\right]\frac{1}{e^{\frac{h(\nu_i-\nu_j)}{kT}}-1}$$

In those equations:

$\alpha(\nu_i)$	Attenuation;
$P_f(z,\nu_i)$	Forward power at frequency ν_i at distance z;
$P_b(z,\nu_i)$	Backward power at frequency ν_i at distance z;
$\gamma(\nu_i)$	Rayleigh scattering coefficient;
$g_R(\nu_j,\nu_i)$	Raman gain coefficient between frequencies ν_i and ν_j
A_{eff}	Effective area of the fiber

V_i Group velocity of pump or signal or ASE noise, which is at frequency v_i

To understand pump-to-pump, signal-to-signal, pump-to-signal interactions, we separate the Equation (3.1) for pumps, ASE noise, and signals:

1. Pump power equations:

$$\frac{dP_f(z,v_i)}{dz} = -\alpha(v_i)P_f(z,v_i) + \gamma(v_i)P_b(z,v_i) + P_f(z,v_i)\sum_j^{v_j>v_i}\frac{g_R(v_j,v_i)}{A_{eff}(v_j,v_i)}\left([P_f(z,v_j)+P_b(z,v_j)\right] - P_f(z,v_i)\sum_j^{v_j<v_i}\frac{v_j}{v_i}\frac{V_j}{V_i}\frac{g_R(v_i,v_j)}{A_{eff}(v_i,v_j)}\left[(P_f(z,v_j)+P_b(z,v_j)\right] \quad (3.2a)$$

$$\frac{dP_b(z,v_i)}{dz} = -\alpha(v_i)P_b(z,v_i) + \gamma(v_i)P_f(z,v_i) + P_b(z,v_i)\sum_j^{v_j>v_i}\frac{g_R(v_j,v_i)}{A_{eff}(v_j,v_i)}\left([P_f(z,v_j)+P_b(z,v_j)\right] - P_b(z,v_i)\sum_j^{v_j<v_i}\frac{v_j}{v_i}\frac{V_j}{V_i}\frac{g_R(v_i,v_j)}{A_{eff}(v_i,v_j)}\left[(P_f(z,v_j)+P_b(z,v_j)\right] \quad (3.2b)$$

The third term is the Raman gain. For the pumps, only Raman gain from other pumps is included. The ASE noise induced gain is noise. Therefore, the third term is split into two parts:

$$P_f(z,\nu_i)\sum_{j}^{\nu_j>\nu_i}\frac{g_R(\nu_j,\nu_i)}{A_{eff}(\nu_j,\nu_i)}\left([P_f(z,\nu_j)+P_b(z,\nu_j)\right]$$

$$=P_f(z,\nu_i)\sum_{j}^{\nu_j(pumps)>\nu_i}\frac{g_R(\nu_j,\nu_i)}{A_{eff}(\nu_j,\nu_i)}\left([P_f(z,\nu_j)+P_b(z,\nu_j)\right] \tag{3.3a}$$

$$+P_f(z,\nu_i)\sum_{j}^{\nu_j(ASE)>\nu_i}\frac{g_R(\nu_j,\nu_i)}{A_{eff}(\nu_j,\nu_i)}\left([P_f(z,\nu_j)+P_b(z,\nu_j)\right]$$

$$P_b(z,\nu_i)\sum_{j}^{\nu_j>\nu_i}\frac{g_R(\nu_j,\nu_i)}{A_{eff}(\nu_j,\nu_i)}\left([P_f(z,\nu_j)+P_b(z,\nu_j)\right]$$

$$=P_b(z,\nu_i)\sum_{j}^{\nu_j(pumps)>\nu_i}\frac{g_R(\nu_j,\nu_i)}{A_{eff}(\nu_j,\nu_i)}\left([P_f(z,\nu_j)+P_b(z,\nu_j)\right] \tag{3.3b}$$

$$+P_b(z,\nu_i)\sum_{j}^{\nu_j(ASE)>\nu_i}\frac{g_R(\nu_j,\nu_i)}{A_{eff}(\nu_j,\nu_i)}\left([P_f(z,\nu_j)+P_b(z,\nu_j)\right]$$

The second term in Equation (3.3a) and Equation (3.3b) should be included in ASE. The following terms are not included and should be included in ASE noise:

1). Stokes emission (ASE noise)

2). Anti-Stokes emission (ASE noise)

2. Signal power equations

$$\frac{dP_f(z,\nu_i)}{dz} = -\alpha(\nu_i)P_f(z,\nu_i)$$

$$+ P_f(z,\nu_i)\sum_{j}^{\nu_j(pumps)>\nu_i} \frac{g_R(\nu_j,\nu_i)}{A_{eff}(\nu_j,\nu_i)}\left([P_f(z,\nu_j)+P_b(z,\nu_j)\right] \tag{3.4a}$$

$$- P_f(z,\nu_i)\sum_{j}^{\nu_j<\nu_i} \frac{\nu_j}{\nu_i}\frac{V_j}{V_i}\frac{g_R(\nu_i,\nu_j)}{A_{eff}(\nu_i,\nu_j)}\left[(P_f(z,\nu_j)+P_b(z,\nu_j)\right]$$

$$\frac{dP_b(z,\nu_i)}{dz} = -\alpha(\nu_i)P_b(z,\nu_i)$$

$$+ P_b(z,\nu_i)\sum_{j}^{\nu_j(pumps)>\nu_i} \frac{g_R(\nu_j,\nu_i)}{A_{eff}(\nu_j,\nu_i)}\left([P_f(z,\nu_j)+P_b(z,\nu_j)\right] \tag{3.4b}$$

$$- P_b(z,\nu_i)\sum_{j}^{\nu_j<\nu_i} \frac{\nu_j}{\nu_i}\frac{V_j}{V_i}\frac{g_R(\nu_i,\nu_j)}{A_{eff}(\nu_i,\nu_j)}\left[(P_f(z,\nu_j)+P_b(z,\nu_j)\right]$$

Signal-to-signal SRS transfers power from shorter to longer wavelength channels and results in the signal power tilt [9]. Signal-to-signal SRS crosstalk can be considered as Raman gain or noise. In this thesis it is considered as noise, and then the second term in Equation (3.4a) and Equation (3.4b) should be moved to ASE noise. Other terms are not included in Equation (3.4) and are moved to ASE noise:

1). Rayleigh scattering by signals

2). Stokes emission

3). Anti-Stokes emission

3. Forward ASE noise power equation

$$\frac{dP_f(z,v_i)}{dz} = -\alpha(v_i)P_f(z,v_i)$$

$$+\gamma(v_i)P_b(z,v_i)$$

$$+P_f(z,v_i)\sum_{j}^{v_j>v_i}\frac{g_R(v_j,v_i)}{A_{eff}(v_j,v_i)}\left([P_f(z,v_j)+P_b(z,v_j)\right]$$

$$+2hv_i\Delta v\sum_{j}^{v_j>v_i}\frac{g_R(v_j,v_i)}{A_{eff}(v_j,v_i)}\left[P_f(z,v_j)+P_b(z,v_j)\right]\left(1+\frac{1}{e^{\frac{h(v_j-v_i)}{kT}}-1}\right)$$

$$-P_f(z,v_i)\sum_{j}^{v_j<v_i}\frac{v_j}{v_i}\frac{V_j}{V_i}\frac{g_R(v_i,v_j)}{A_{eff}(v_i,v_j)}\left[(P_f(z,v_j)+P_b(z,v_j)\right]$$

$$+2hv_i\Delta v\sum_{j}^{v_j<v_i}\frac{v_j}{v_i}\frac{V_j}{V_i}\frac{g_R(v_i,v_j)}{A_{eff}(v_i,v_j)}\left[(P_f(z,v_j)+P_b(z,v_j)\right]\left(\frac{1}{e^{\frac{h(v_i-v_j)}{kT}}-1}\right)$$

(3.5)

1). If SRS crosstalk between signals is considered as noise, the third term should be included in ASE noise.

2). The fourth and sixth terms should include generated ASE noise by signals and pumps,

4. Backward ASE noise power equation

$$\frac{dP_b(z,v_i)}{dz} = -\alpha(v_i)P_b(z,v_i)$$

$$+\gamma(v_i)P_f(z,v_i)$$

$$+P_b(z,\nu_i)\sum_{j}^{\nu_j>\nu_i}\frac{g_R(\nu_j,\nu_i)}{A_{eff}(\nu_j,\nu_i)}\left([P_f(z,\nu_j)+P_b(z,\nu_j)\right]$$

$$+2h\nu_i\Delta\nu\sum_{j}^{\nu_j>\nu_i}\frac{g_R(\nu_j,\nu_i)}{A_{eff}(\nu_j,\nu_i)}\left[P_f(z,\nu_j)+P_b(z,\nu_j)\right]\left(1+\frac{1}{e^{\frac{h(\nu_j-\nu_i)}{kT}}-1}\right)$$

$$-P_b(z,\nu_i)\sum_{j}^{\nu_j<\nu_i}\frac{\nu_j}{\nu_i}\frac{V_j}{V_i}\frac{g_R(\nu_i,\nu_j)}{A_{eff}(\nu_i,\nu_j)}\left[(P_f(z,\nu_j)+P_b(z,\nu_j)\right]$$

$$+2h\nu_i\Delta\nu\sum_{j}^{\nu_j<\nu_i}\frac{\nu_j}{\nu_i}\frac{V_j}{V_i}\frac{g_R(\nu_i,\nu_j)}{A_{eff}(\nu_i,\nu_j)}\left[(P_f(z,\nu_j)+P_b(z,\nu_j)\right]\left(\frac{1}{e^{\frac{h(\nu_i-\nu_j)}{kT}}-1}\right)$$

(3.6)

1). If SRS crosstalk between signals is considered as noise, the third term should be included in ASE noise.

2). If MPI is included, the second term should be included in ASE noise

3). The fourth and sixth terms should include generated ASE noise by signals and pumps,

To apply those differential equations to a FRA with length L, the fiber can be separated into n sections. Each section is an elemental amplification section and has a length of $\Delta z = \frac{L}{n}$, where Δz is the step size. With the increase of section number n, the step size is smaller and calculation accuracy is improved. However, the section number n cannot be increased unlimitedly, since the computation time is also increased. Figure 3.2 gives the evolution of a transmission fiber for the forward direction.

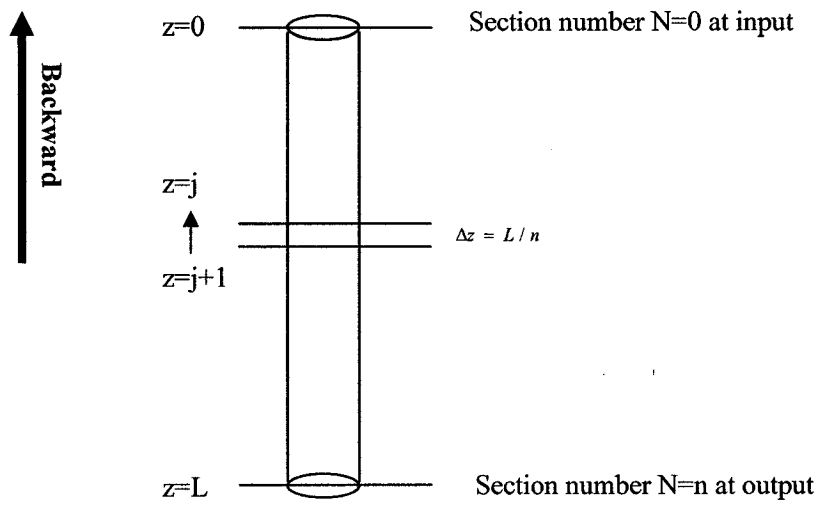

Figure 3.2 - The illustration of a transmission fiber of n sections for the backward propagation direction

The calculation process is simply described [28][29] as follows:

Step 1, Boundary conditions are set for input power $P_f(0,v_p)$ and $P_f(0,v_s)$ at the position of $z=0$, and $P_b(L,v_p)$ at the position of $z=L$. ASE noise is typically set as $P_f(0,v_{ASE})=0$ and $P_b(L,v_{ASE})=0$.

Step 2, The calculation loop begins at z_{n-1} for the backward propagation direction. The evolution is illustrated in Figure 3.2. $P_b(z_j,v_i)$ is obtained by solving the backward propagation Equation (3.1b) at the point $z=j+1$ according to Rung-Kutta 4th-order method. As a result, the backward optical power is obtained at each of the point $z_{n-1}, z_{n-2}.....z_0$.

Step 3, The calculation loop begins at z_1 for the forward propagation direction. The evolution is illustrated in Figure 3.3. $P_f(z_{j+1}, v_i)$ can be obtained by solving the forward propagation Equation (3.1a) at the point $z = j$ according to Rung-Kutta 4th-order method. As a result, the forward optical power is obtained at each of the point $z_1, z_2 \ldots\ldots z_n$. A calculation loop is over.

Step 4, Justify whether the simulated transmission system is steady. Only if the results of the last two loops are the same, which is measured by the difference of the results, the calculation is finished. Otherwise, repeat the step 2, step 3 and step 4.

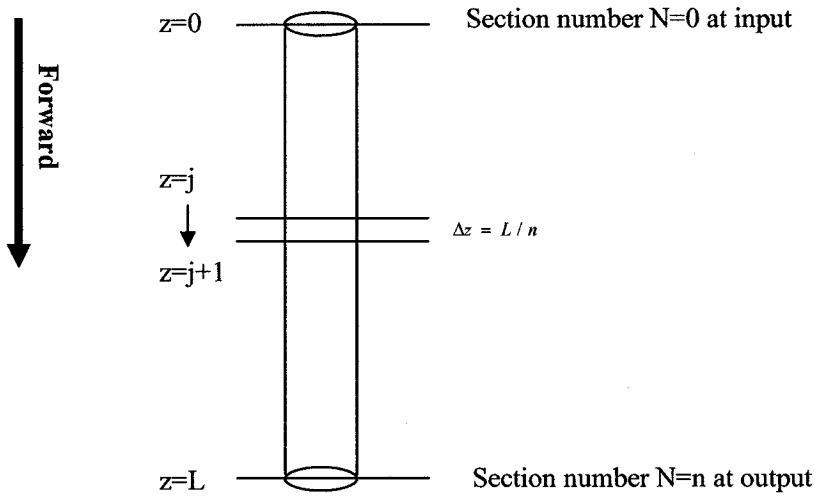

Figure 3.3 - The illustration of a transmission fiber of n sections for the forward propagation direction

In order to check the validity of our model, we repeat the same simulations as given in [26]. The 1^{st} simulation in [26] is based on the fiber loss and Raman gain, as well as the Rayleigh backscattering coefficient measured for 13-km Lucent TrueWave RS transmission fiber at room temperature. The fiber is pumped with 13 mW at 1560 nm. To verify this simulation, we use 13-km TrueWave Reach transmission fiber and the other configuration is the same. Figure 3.4 is the illustration of power density from [26] and our simulation. The results from [26] and our simulation have the same power density shape but with different absolute values due to different fibers.

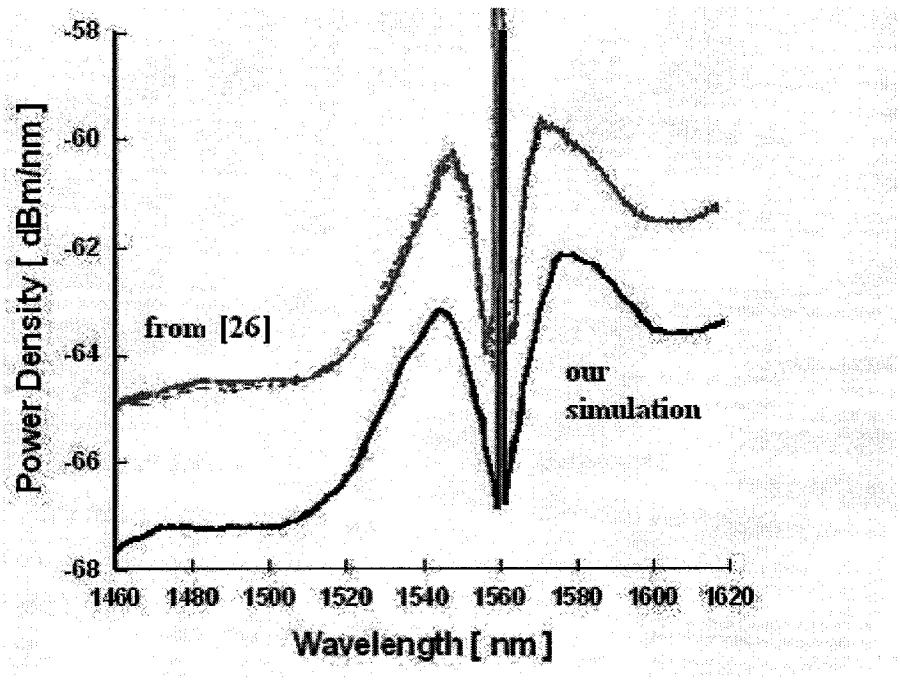

Figure 3.4 - Power density comparison between the result from [26] and our simulation

The 2^{nd} simulation is based on 100 km span of Corning SMF-28 with 51 channels in the C-band (1529.55-1569.59). The total input signal power is 20 dBm with flat channel

distribution. A pair of co propagating pumps at 1430 nm and 1454 nm with powers of 300 and 262.5 mW, respectively, is used. Moreover, SRS between signals is considered as noise and MPI is not considered according to [26]. Figure 3.5 shows the comparison of on-off gain between [26] and our simulation. Gain spectra in Figure 3.5 are completely the same except that the gain from our simulation is about 1 dB smaller than the gain from [26]. The difference in the absolute gain values may be due to the different gain scaling methods. We do not have the same g_R as in [26] and our scaling method is descried in Section 3.2. Therefore, we confirmed the correctness of our modeling.

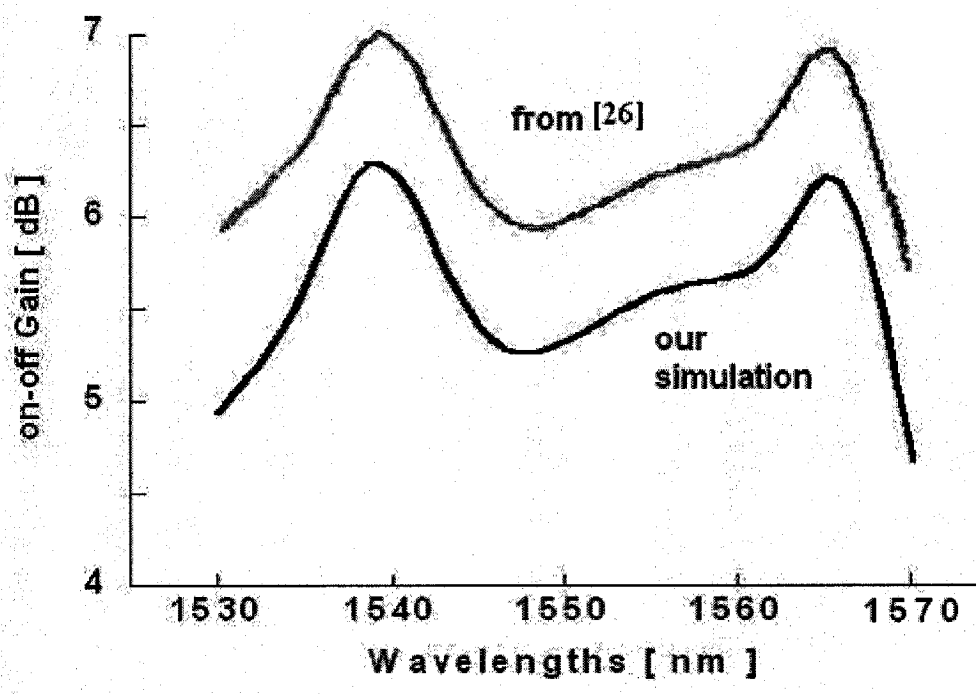

Figure 3.5 - On-off gain comparison between the result from [26] and our simulation. SRS between signals is noise and MPI is not considered

3.2 Scaling of the Raman Gain Coefficient

In this section, we consider a fundamental parameter for Raman amplification: the Raman gain coefficient. This parameter determines the strength of the coupling between a pump beam and a signal beam due to SRS.

For a given fiber, Raman gain spectra are fixed for a single pump wavelength. However, the coefficients $g_R(\lambda_p, \Delta\nu)$ are not the same for different pump wavelengths with the same $\Delta\nu$. In [22] a new method about how to predict Raman gain coefficient is demonstrated. This method is helpful for designing broadband Raman amplifiers that have many pumps covering a range of wavelengths; the Raman gain coefficient only needs to be measured at a single wavelength if one has measurements or predictions for the effective area versus wavelength.

The Equation (3.7) shows the relationship of reference pump ν_p, new pump ν_m, effective area A_{eff}, and normalized gain coefficient $\bar{g}_R$, which is equal to g_R / A_{eff}.

$$\bar{g}_R(\nu_m, \Delta\nu) = \bar{g}_R(\nu_p, \Delta\nu)\frac{\nu_m - \Delta\nu}{\nu_p - \Delta\nu} \times \frac{A_{eff}(\nu_p) + A_{eff}(\nu_p - \Delta\nu)}{A_{eff}(\nu_m) + A_{eff}(\nu_m - \Delta\nu)} \tag{3.7}$$

Here, $\Delta\nu = \nu_m - \nu_s$ is the frequency difference between a new pump and a signal.

The following measurement results illustrate the validity of this approach. Figure 3.6 shows the measured Raman gain coefficient of TrueWave-RS fiber for four pump wavelengths: 1425, 1455, and 1485 nm. We use Equation (3.7) to obtain each Raman gain coefficient curve from their original pump wavelengths to the new pump

wavelengths of 1425, 1455, and 1485 nm. To confirm the validity of Raman gain scaling in this thesis, our calculations for TrueWave-Reach fiber are shown in Figure 3.7. Since not all parameters of TrueWave-RS fiber are available, TrueWave-Reach fiber is used in this thesis. The gain coefficients in Figure 3.6 and Figure 3.7 have the same shape, which confirms that our calculations are correct.

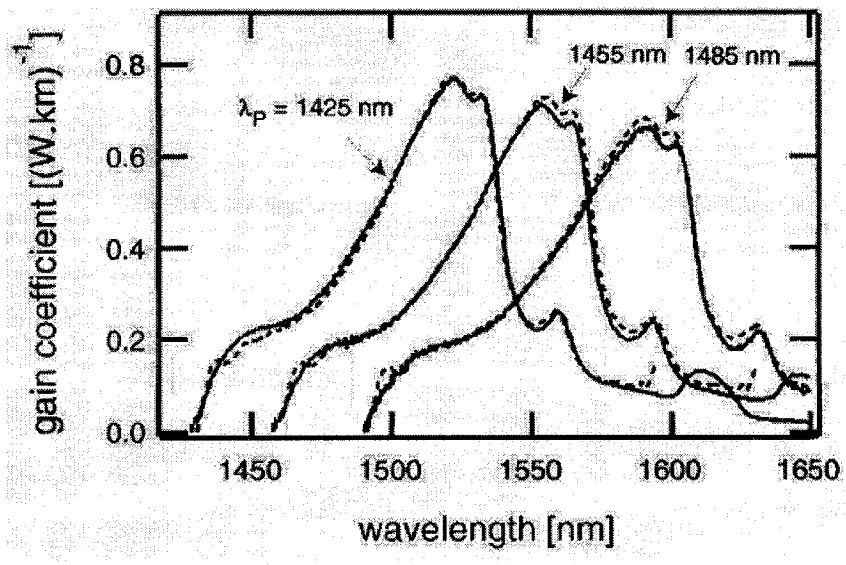

Figure 3.6 - Predicted (dashed curves) and measured (solid curves) Raman gain spectra on a TrueWave-RS fiber from [22]

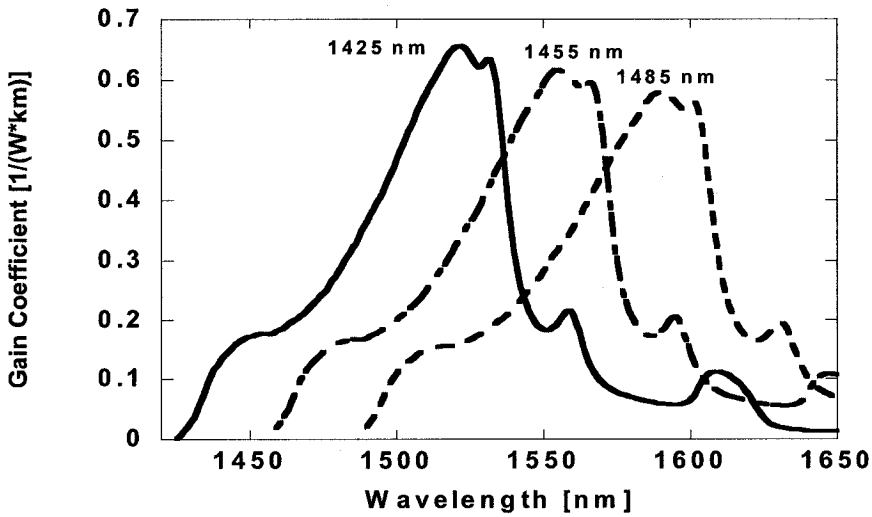

Figure 3.7 - Raman gain coefficient scaling for TrueWave-Reach fiber.

CHAPTER 4 MODELING OF INCOHERENT PUMPING SOURCES

This chapter mainly focuses on the mechanism and modeling of high-power incoherent pumps. How the incoherent pump was produced is presented in Section 4.1. This was achieved through coupling of a low-power seed optical signal from a semiconductor ASE source into a long-cavity semiconductor amplifier waveguide [19]. The numerical incoherent pump model is introduced in Section 4.2.

4.1 Mechanism of high-power incoherent pumps

FRAs have attracted much attention as they have many inherent advantages over their EDFA counterparts [19]. Broader and flatter gain spectra with lower NF can be achieved at center wavelength covering C-Band, L-Band and even S-band. On the other hand, FRAs performance suffers from limitations imposed by today's high-power pump laser technology. The ability to create modules with more than 450 mW of broadband pump light allows us to address many of these FRA limitations in a fundamental manner.

Traditionally, to reduce the polarization dependent gain, each pump wavelength requires light to be launched at two orthogonal linear polarizations. The introduction of incoherent pumping completely eliminates the polarization dependency. High-power and spectrally incoherent semiconductor pump sources rather than traditional laser sources were achieved through coupling of a low-power seed optical signal from a semiconductor ASE source into a long-cavity semiconductor amplifier waveguide which was optimized

in design for CW power amplification. This seeded power-optical-amplifier (SPOA) concept relies on the design and fabrication semiconductor optical amplifiers. The resulting SPOA output can be efficiently coupled to SMF-28 fiber with a loss of <0.8 dB. Figure 4.1 [23] illustrates a photograph of a high-power and broad bandwidth Raman pump module. The output spectrum at 100 mW of optical power is shown in Figure 4.2 [23].

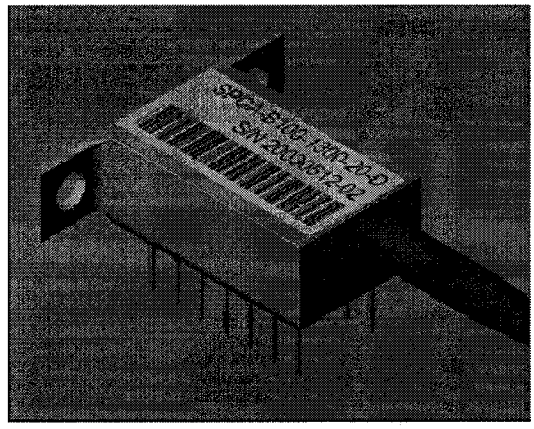

Figure 4.1 - High power broadband Raman pump module

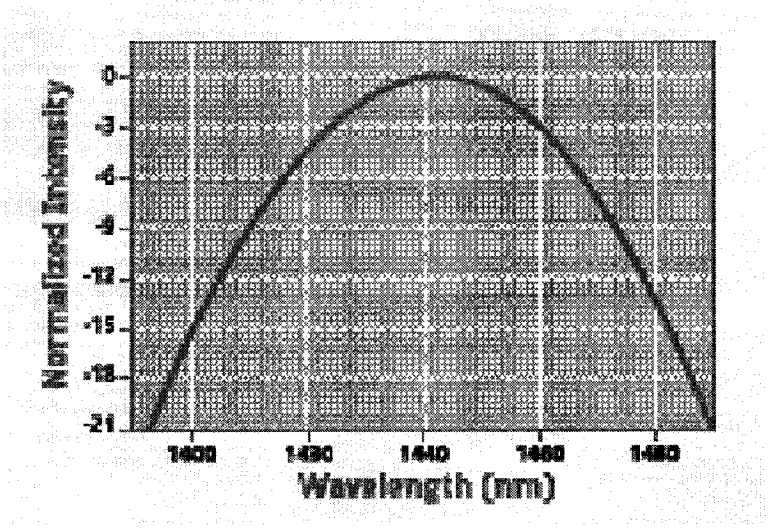

Figure 4.2 - The optical spectrum of the broadband Raman pump module at an output power of 100 mW

4.2 Modeling

The modeling of the incoherent pumping sources is briefly described as follows:

Step 1. We use the commercial available function to generate Gaussian noise in a 200 nm broad bandwidth. Then the intensity of the generated Gaussian noise is adjusted by ASE variance. Broadband ASE noise is generated

Step 2. Let the generated broadband ASE noise pass through a Gaussian optical filter. The shape of the filter can be adjusted by the FWHM and center wavelength. The referring Gaussian filter equation is given by

$$H(\lambda) = \exp\left[-\frac{1}{2}\frac{(\lambda-\lambda_c)^2}{\lambda_0^{\,2}}\right] \tag{4.1}$$

Where, λ_c is the center wavelength and

$$\lambda_0 = \frac{FWHM}{\sqrt{2\ln 2}}. \tag{4.2}$$

Step 3. An incoherent pump, whose spectrum is Gaussian-intensity distributed, is generated.

An example of one incoherent pump is shown in Figure 4.3. The filter is centered at 1425 nm and FWHM is 35 nm. Total power is 666 mW and the spectrum spreads from 1361 nm to 1486 nm. Figure 4.4 shows the gain after an 8 km DCF fiber, which is counter-pumped by the above incoherent pump and its average gain is 20 dB.

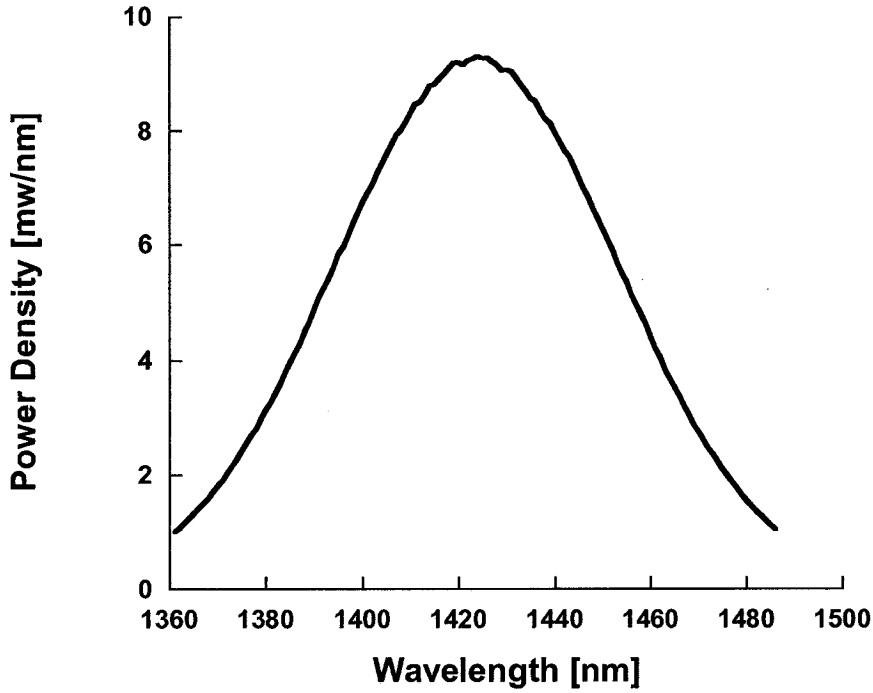

Figure 4.3 - An example of an incoherent pump centered at 1425 nm with a FWHM of 35 nm

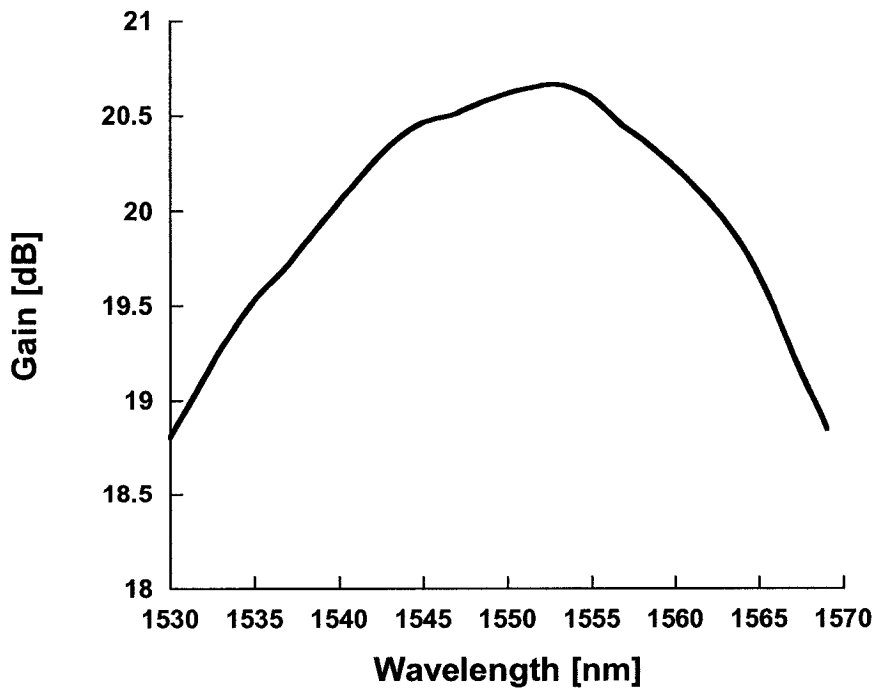

Figure 4.4 – Raman gain of a 666 mW incoherent pump for an 8 km DCF fiber

CHAPTER 5 PERFORMANCE COMPARISON OF C-BAND DISFRAs WITH INCOHERENT PUMPING TO COHERENT PUMPING

In this chapter, the performance of C-band DisFRAs with incoherent pumping is investigated and compared to conventional coherent pumping. All comparisons in this chapter are based on the same parameters: a fiber length of 8 km with the fiber type of OFS-DCF, 40 signal channels with channel spacing of 125 GHz over the spectrum of from 1530 to 1570 nm, -20 dBm per channel for input power and the average gain of 20 dB. In our analysis, we always optimize the pumping wavelengths of pumping sources for C-band DisFRAs to realize the gain as flat as possible.

C-band DisFRAs with counter-pumping are analyzed in Section 5.1 and with co-pumping are analyzed in Section 5.2. In these two sections, we separately explore the relationship of gain ripple, average NF, NF ripple, average OSNR, OSNR ripple and pumping efficiency with FWHM of an incoherent pumping source and compare the performance of C-band DisFRAs with multiple incoherent pumping sources to multiple coherent pumping sources. The performance of C-band DisFRAs with incoherent co-pumping is compared to incoherent counter-pumping in Section 5.3. The simulation results show that C-band DisFRAs with incoherent co-pumping are superior to incoherent counter-pumping due to flatter NF and OSNR, lower NF, higher OSNR and increased pumping efficiency.

5.1 C-band DisFRAs with counter-pumping

This section focuses on C-band DisFRAs with counter-pumping. We first consider one counter-pumping source [30]. We optimize an incoherent counter-pumping source with a FWHM of from 0 to 35 nm to realize the flattest gain and the optimal pumping wavelengths ranged from 1455 to 1425 nm.

In order to understand the influence of FMHM of an incoherent counter-pumping source on DisFRAs, we explore the relationship of gain ripple, average NF, NF ripple, average OSNR, OSNR ripple and pumping efficiency with FWHM of an incoherent counter-pumping source. The coherent pumping is considered as a special case of incoherent pumping, i.e., FWHM = 0. The detailed simulation results are listed in Table 5.1.

Increasing the spectral bandwidth of the incoherent pumping source, gain ripple, NF ripple, and OSNR ripple decrease exponentially in dB. Figure 5.1 (a) shows the gain ripple, average NF, NF ripple, average OSNR, and OSNR ripple as a function of FWHM of the incoherent pumping source for C-band DisFRAs. The average NF and OSNR keep almost unchanged for the FWHM of from 0 to 35 nm due to the same average gain.

Pumping power increases exponentially in mW with the increase of FWHM of the incoherent pumping source. Pumping power is shown separately in Figure 5.1 (b) for the incoherent pumping with a FWHM of from 0 to 35 nm. The pumping efficiency is reduced with the increase of FWHM of the incoherent pumping source due to the fact that a larger portion of incoherent pumping power contributes to the Raman amplification

for the spectrum of outside the C-band.

Table 5.1 Detailed simulation results for C-band DisFRAs with one incoherent counter-pumping source.

One incoherent counter-pumping source with a FWHM of from 0 to 35 nm								
FWHM [nm]	0	5	10	15	20	25	30	35
C.W. [nm]	1455	1454	1451	1450	1445	1440	1435	1425
Power [mW]	500	511	525	551	580	614	641	666
Gain ripple [dB]	9.3	8.5	7.1	5.5	3.7	2.8	2.6	1.9
Average NF [dB]	6.3	6.3	6.1	6.0	6.0	6.0	6.0	6.0
NF ripple [dB]	3.5	3.4	2.8	2.1	1.7	1.5	1.2	1.1
Average OSNR [dB]	21.7	21.7	22.0	22.0	22.0	22.0	22.0	22.0
OSNR ripple [dB]	3.6	3.5	2.9	2.1	1.8	1.6	1.2	1.1

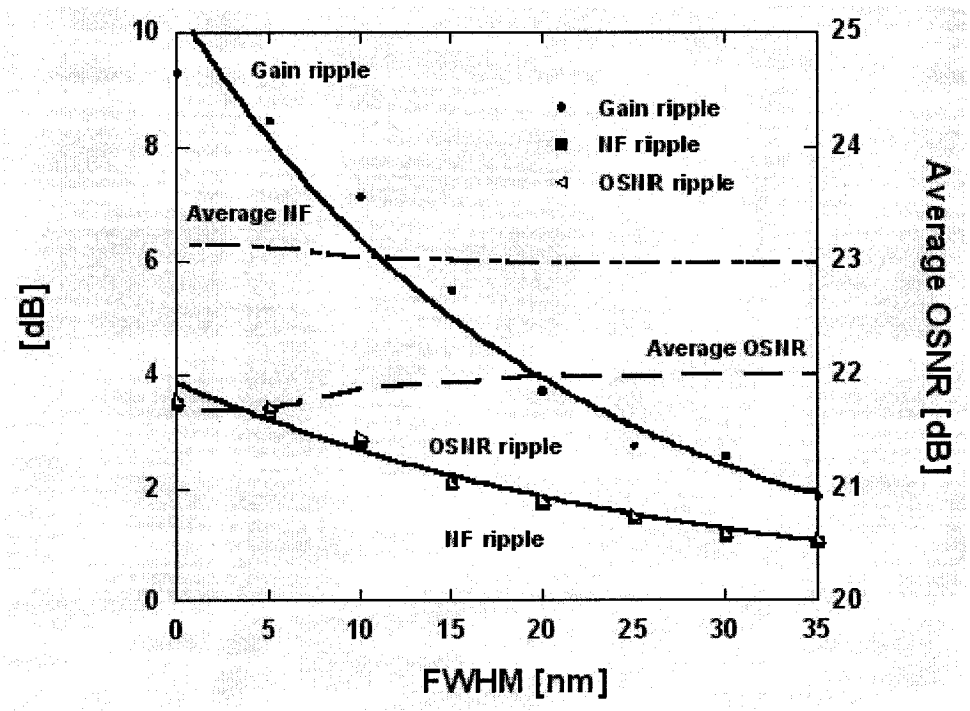

(a)

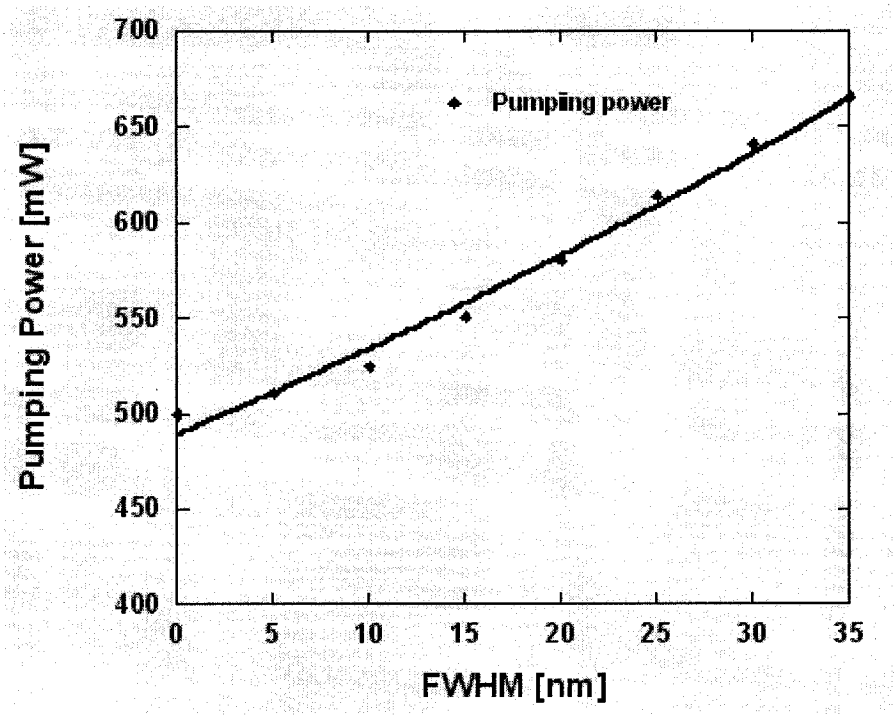

(b)

Figure 5.1 - The performance of C-band DisFRAs with one incoherent counter-pumping source. (a) Gain ripple, average NF, NF ripple, average OSNR, and OSNR ripple and (b) Pumping power. Solid lines represent exponential curves.

In the above analysis, only one pumping source was used for C-band DisFRAs. We extend our study using multiple incoherent counter-pumping sources in the following. We consider C-band DisFRAs with two incoherent counter-pumping sources [30]. By optimization of pumping wavelengths to obtain the flattest gain, it is found that the incoherent pumping sources should have a center wavelength at 1427 nm and the other wavelength at 1469 nm, both with a FWHM of 15 nm. For comparison, we also optimized C-band DisFRAs with two or four coherent counter-pumping sources. The

simulation results are listed in Table 5.2. Figure 5.2 shows the gain, NF, and forward noise power spectra for DisFRAs with coherent or incoherent pumping.

The gain ripple is 1.8, 0.7 and 0.3 dB, the average NF is 5.9, 6.0 and 6.0 dB, the NF ripple is 1.2, 1.0, 1.0 dB, the average OSNR is 22.1, 22.0 and 21.9 dB, and the OSNR ripple is 1.3, 1.1, and 1.1 dB for DisFRAs with two, four coherent counter-pumping sources and two incoherent counter-pumping sources, respectively. The reduced gain ripple suggests that DisFRAs with incoherent counter-pumping sources have significantly flatter gain. The average NF and OSNR for DisFRAs with incoherent pumping are similar to coherent pumping due to the same average gain. The NF flatness and the OSNR flatness by using incoherent pumping are also similar to coherent pumping. As seen in Figure 5.2 (b), the noise performance by using incoherent pumping is slightly degraded at the shorter wavelengths (1530-1545 nm). To understand that behavior, calculated forward noise spectra for the above three cases are illustrated in Figure 5.2 (c). The higher forward noise power at shorter wavelengths contributes to the NF increase. As we have mentioned in Section 2.2, MPI and single-pass reflected noise degrades the noise performance of DisFRAs. The noise degradation increases with gain due to MPI. Almost all the single-pass reflected noise has the larger gain at the amplifier output end for DisFRAs with counter-pumping compared to co-pumping [1].

The pumping power is 576, 631 and 691 mW for DisFRAs with two, four coherent counter-pumping sources and two incoherent counter-pumping sources, respectively. Pumping efficiency is decreased for incoherent pumping due to the fact that a larger

portion of pumping power contributes to the Raman amplification for the spectrum of outside the C-band (i.e. ASE noise).

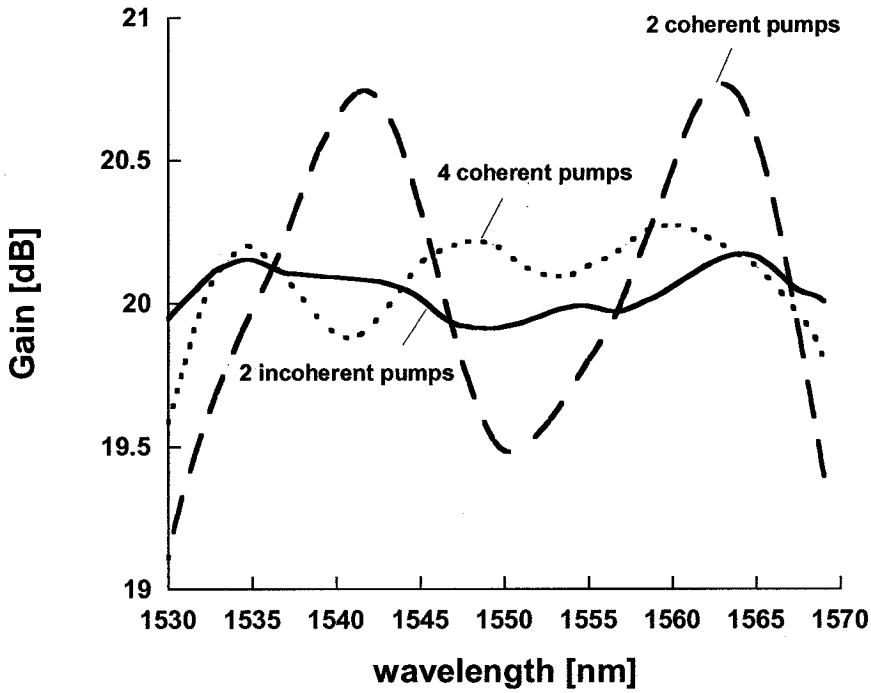

(a)

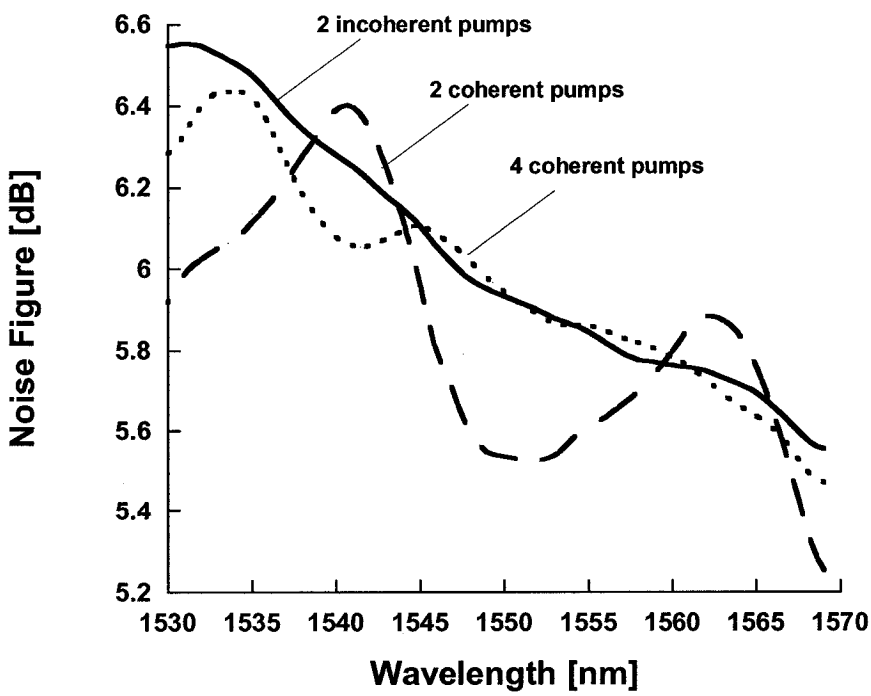

(b)

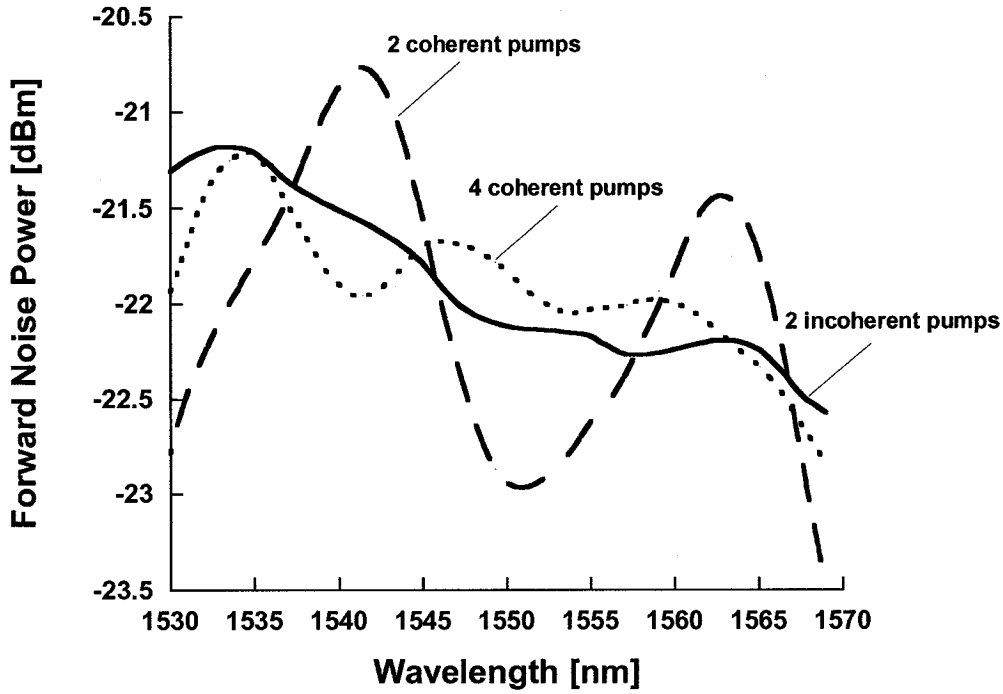

(c)

Figure 5.2 - (a) Gain, (b) NF, and (c) Forward noise power spectrum for C-band DisFRAs with two, or four coherent counter-pumping sources or two incoherent counter-pumping sources.

Table 5.2 Detailed simulation results for C-band DisFRAs with multiple counter-pumping sources.

<table>
<tr><th colspan="10">Multiple coherent or incoherent counter-pumping sources</th></tr>
<tr><td rowspan="11">Pump</td><td colspan="3">2 Incoherent pumps</td><td colspan="3">2 Coherent pumps</td><td colspan="3">4 Coherent pumps</td></tr>
<tr><td colspan="2">Total power [mW]</td><td>691</td><td colspan="2">Total power [mW]</td><td>576</td><td colspan="2">Total power [mW]</td><td>631</td></tr>
<tr><td rowspan="2">1</td><td>FWHM [nm]</td><td>15</td><td rowspan="2">1</td><td>Power [mW]</td><td>380</td><td rowspan="2">1</td><td>Power [mW]</td><td>270</td></tr>
<tr><td>C.W. [nm]</td><td>1427</td><td>C.W. [nm]</td><td>1435</td><td>C.W. [nm]</td><td>1428</td></tr>
<tr><td rowspan="2">2</td><td>FWHM [nm]</td><td>15</td><td rowspan="2">2</td><td>Power [mW]</td><td>196</td><td rowspan="2">2</td><td>Power [mW]</td><td>160</td></tr>
<tr><td>C.W. [nm]</td><td>1469</td><td>C.W. [nm]</td><td>1464</td><td>C.W. [nm]</td><td>1439</td></tr>
<tr><td colspan="3" rowspan="4"></td><td colspan="3" rowspan="4"></td><td rowspan="2">3</td><td>Power [mW]</td><td>146</td></tr>
<tr><td>C.W. [nm]</td><td>1459</td></tr>
<tr><td rowspan="2">4</td><td>Power [mW]</td><td>55</td></tr>
<tr><td>C.W. [nm]</td><td>1479</td></tr>
<tr><td>Gain ripple [dB]</td><td colspan="3">0.3</td><td colspan="3">1.8</td><td colspan="3">0.7</td></tr>
<tr><td>Average NF [dB]</td><td colspan="3">6.0</td><td colspan="3">5.9</td><td colspan="3">6.0</td></tr>
<tr><td>NF ripple [dB]</td><td colspan="3">1.0</td><td colspan="3">1.2</td><td colspan="3">1.0</td></tr>
<tr><td>Average OSNR [dB]</td><td colspan="3">21.9</td><td colspan="3">22.1</td><td colspan="3">22.0</td></tr>
<tr><td>OSNR ripple [dB]</td><td colspan="3">1.1</td><td colspan="3">1.3</td><td colspan="3">1.1</td></tr>
</table>

5.2 C-band DisFRAs with co-pumping

This section focuses on C-band DisFRAs with co-pumping. We first consider one pumping source [30]. We optimize an incoherent pumping source with a FWHM of from 0 to 35 nm to realize the flattest gain and the optimal pumping wavelengths ranged from 1455 to 1425 nm.

In order to understand the influence of FMHM of an incoherent co-pumping source on DisFRAs, we explore the relationship of gain ripple, average NF, NF ripple, average OSNR, OSNR ripple and pumping efficiency with FWHM of an incoherent co-pumping source. The coherent pumping is considered as a special case of incoherent pumping, i.e., FWHM = 0. The detailed simulation results are listed in Table 5.3.

Increasing the spectral bandwidth of the incoherent pumping source, gain ripple, NF ripple and OSNR ripple decrease exponentially in dB. Figure 5.3 (a) shows the gain ripple, average NF, NF ripple, average OSNR, and OSNR ripple as a function of FWHM of the incoherent pumping source for C-band DisFRAs. The average NF and OSNR keep almost unchanged for the FWHM of from 0 to 35 nm due to the same average gain.

Pumping power increases exponentially in mW with the increase of FWHM of the incoherent pumping source. Pumping power is shown separately in Figure 5.3 (b) for the incoherent pumping with a FWHM of from 0 to 35 nm. The pumping efficiency is reduced with the increase of FWHM due to the fact that a larger portion of incoherent pumping power contributes to the Raman amplification for the spectrum of outside the C-band.

Table 5.3 Detailed simulation results for C-band DisFRAs with one incoherent co-pumping source

One incoherent co-pumping source with a FWHM of from 0 to 35 nm								
FWHM [nm]	0	5	10	15	20	25	30	35
C.W. [nm]	1455	1454	1451	1450	1445	1440	1435	1425
Power [mW]	450	460	480	501	534	568	600	626
Gain ripple [dB]	9.4	8.5	7.3	5.2	4.1	3.2	2.3	2.2
Average NF [dB]	5.7	5.7	5.6	5.4	5.4	5.4	5.5	5.5
NF ripple [dB]	3.1	2.9	2.5	1.8	1.4	1.2	0.9	0.8
Average OSNR [dB]	22.2	22.3	22.4	22.6	22.6	22.5	22.5	22.4
OSNR ripple [dB]	3.2	3.0	2.6	1.8	1.5	1.3	1.0	0.9

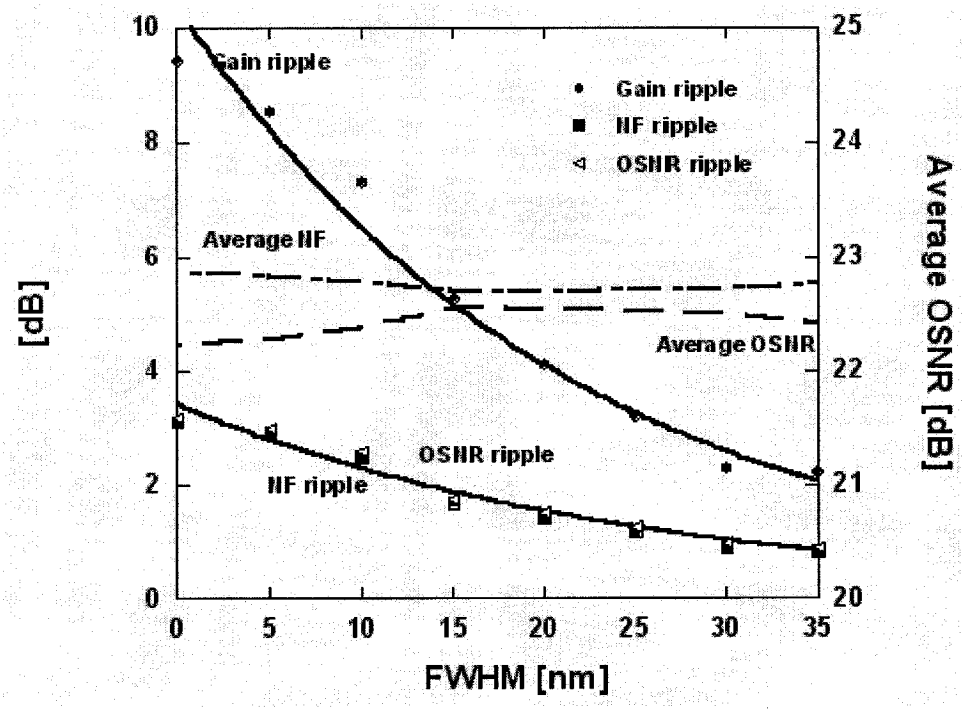

(a)

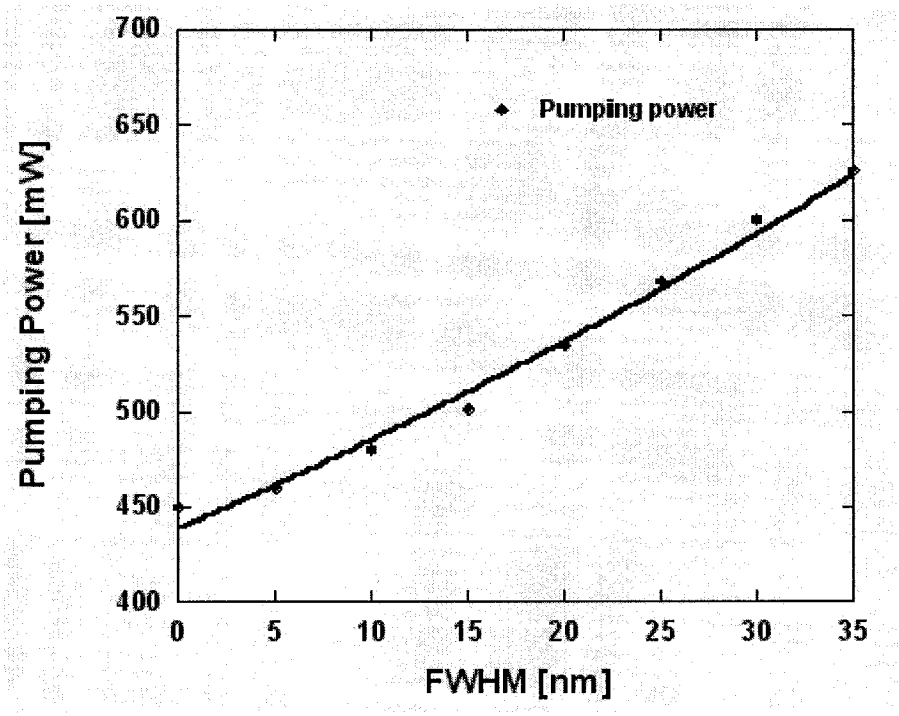

(b)

Figure 5.3 - The performance of C-band DisFRAs with one incoherent co-pumping source. (a) Gain ripple, average NF, NF ripple, average OSNR, and OSNR ripple and (b) Pumping power. Solid lines represent exponential curves.

In the above analysis, only one pumping source was used. We extend our study using multiple pumping sources in the following. By optimization of two pumping wavelengths to obtain the flattest gain, it is found that the incoherent pumping sources should have a center wavelength at 1427 nm and the other wavelength at 1469 nm, both with a FWHM of 15 nm. For comparison, we also optimized DisFRAs with two or four coherent pumping sources. Figure 5.4 shows the gain, NF, and OSNR for DisFRAs with coherent or incoherent pumping. Simulation results are listed in Table 5.4.

The gain ripple is 1.7, 0.7 and 0.3 dB, the average NF is 5.3, 5.4, and 5.4 dB, the NF ripple is 0.7, 0.3, and 0.2 dB, the average OSNR is 22.6, 22.6 and 22.6 dB, and the OSNR ripple is 0.8, 0.3, and 0.2 dB for DisFRAs with two, four coherent pumping sources and two incoherent pumping sources, respectively. It is shown in Figure 5.4 (a) that DisFRAs with two incoherent co-pumping sources have significantly flatter gain compared to two or four coherent pumping sources. The average NF and OSNR for DisFRAs with incoherent pumping are similar to coherent pumping due to the same average gain. Both the NF flatness and the OSNR flatness are improved for DisFRAs with incoherent pumping compared to coherent pumping. As seen in Figure 5.4 (b), the NF spectrum resembles the gain spectrum in Figure 6.4 (a). Because of MPI, the noise degradation increases with gain. Reflected noise has almost no impact on forward pumped amplifiers because most of the reflected noise does not have the high gain close to the fiber output end [1].

The pumping power is 530, 558 and 574 mW for two, or four coherent pumping sources or two incoherent pumping sources. Pumping efficiency is decreased for DisFRAs with incoherent pumping due to the fact that a larger portion of pumping power contributes to the Raman amplification for the spectrum of outside the C-band (i.e. ASE noise).

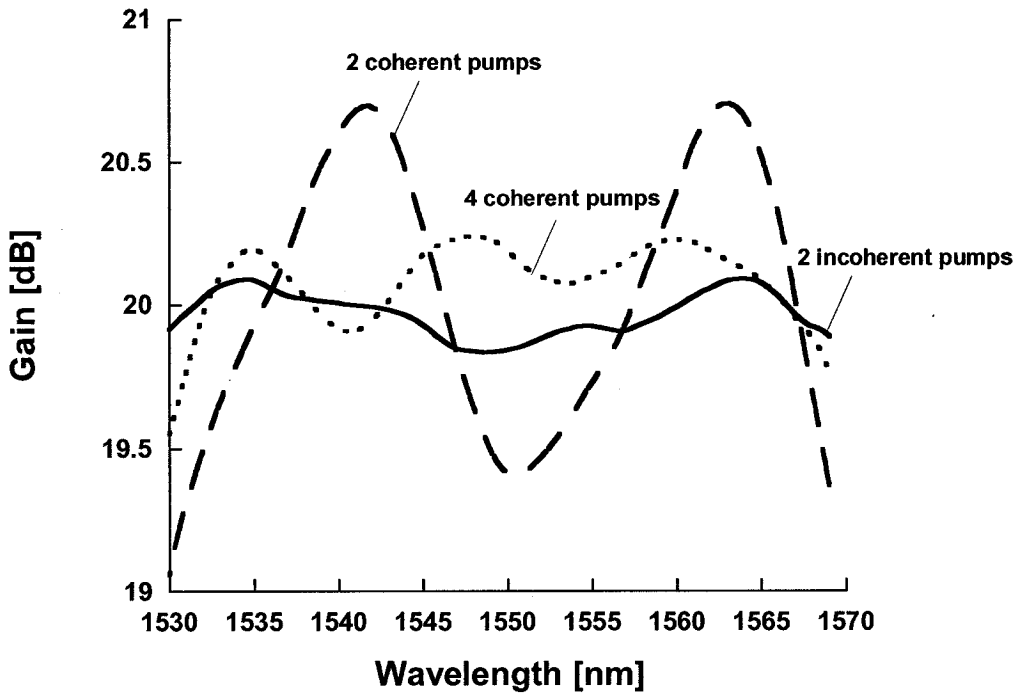
21
20.5
20
19.5
19
Gain [dB]
2 coherent pumps
4 coherent pumps
2 incoherent pumps
1530 1535 1540 1545 1550 1555 1560 1565 1570
Wavelength [nm]

(a)

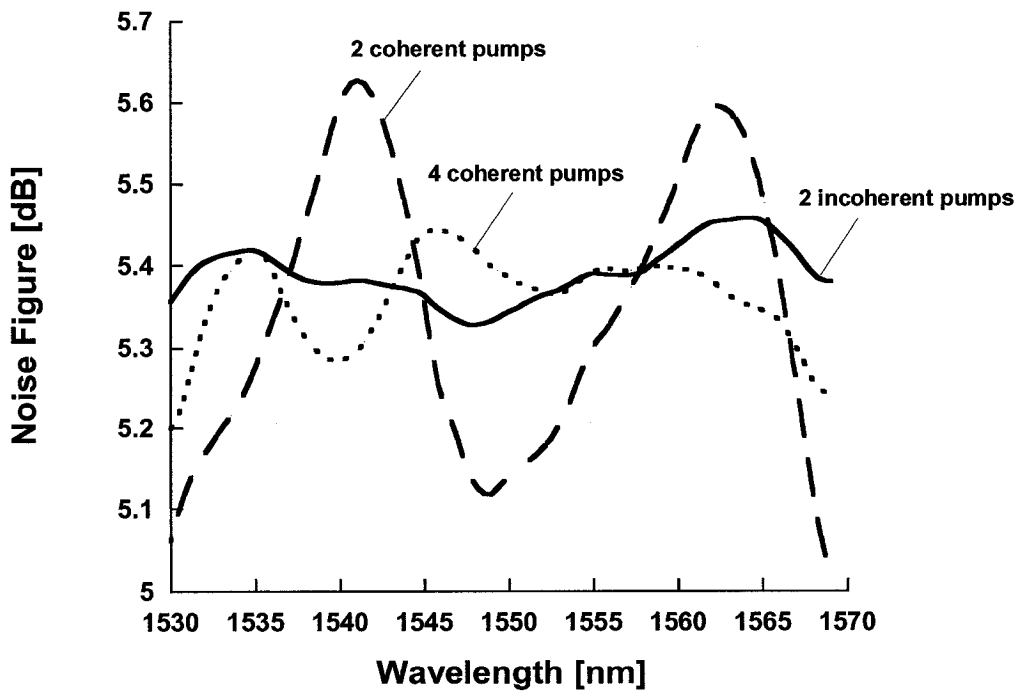
5.7
5.6
5.5
5.4
5.3
5.2
5.1
5
Noise Figure [dB]
2 coherent pumps
4 coherent pumps
2 incoherent pumps
1530 1535 1540 1545 1550 1555 1560 1565 1570
Wavelength [nm]

(b)

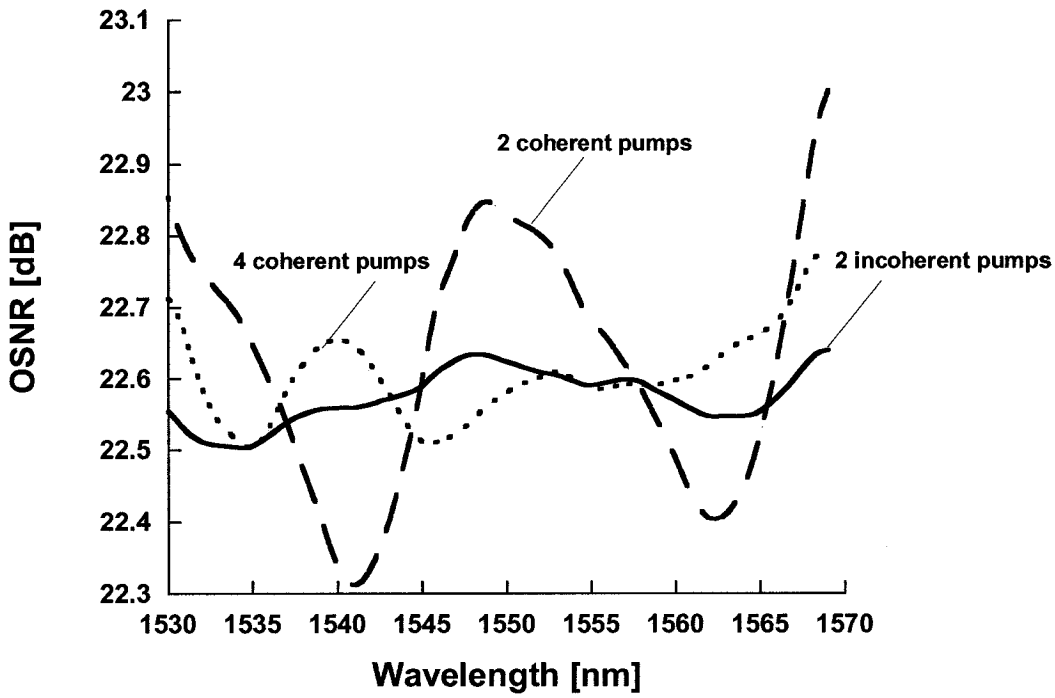

(c)

Figure 5.4 - (a) Gain, (b) NF, and (c) OSNR of C-band DisFRAs with two, or four coherent co-pumping sources or two incoherent co-pumping sources

Table 5.4 Detailed simulation results for C-band DisFRAs with multiple co-pumping sources

Multiple coherent or incoherent co-pumping sources												
Pump	2 Incoherent pumps			2 Coherent pumps			4 Coherent pumps		
	Total power [mW]		643	Total power [mW]		530	Total power [mW]		574
	1	FWHM [nm]	15	1	Power [mW]	340	1	Power [mW]	224
		C.W. [nm]	1427		C.W. [nm]	1435		C.W. [nm]	1428
	2	FWHM [nm]	15	2	Power [mW]	190	2	Power [mW]	152
		C.W. [nm]	1469		C.W. [nm]	1464		C.W. [nm]	1439
							3	Power [mW]	141
								C.W. [nm]	1459
							4	Power [mW]	57
								C.W. [nm]	1479
Gain ripple [dB]	0.3			1.7			0.7		
Average NF [dB]	5.4			5.3			5.4		
NF ripple [dB]	0.2			0.7			0.3		
Average OSNR [dB]	22.6			22.6			22.6		
OSNR ripple [dB]	0.2			0.8			0.3		

5.3 The performance comparison of C-band DisFRAs with incoherent co-pumping to incoherent counter-pumping

This section focuses on the performance comparison of C-band DisFRAs with incoherent co-pumping to incoherent counter-pumping. The simulation results are in Table 5.5. Figure 5.5 shows the gain ripple, average NF, NF ripple, average OSNR and OSNR ripple spectra for DisFRAs with one incoherent pumping source.

It is shown in Figure 5.5 (a) that the gain flatness for DisFRAs with incoherent co-pumping is similar to incoherent counter-pumping. The average NF for DisFRAs with incoherent co-pumping is improved about 0.59 dB compared to incoherent counter-pumping. The NF is degraded for DisFRAs with incoherent counter-pumping since almost all the single-pass reflected noise obtains the larger gain at the amplifier output end compared to incoherent co-puming. Reflected noise has almost no impact on forward pumped amplifiers because most of the reflected noise does not have the high gain close to the fiber output end. The average OSNR for DisFRAs with incoherent co-pumping is increased 0.60 dB compared to incoherent counter-pumping. The NF flatness is improved 0.33 dB and the OSNR flatness is improved 0.36 dB for DisFRAs with incoherent co-pumping compared to incoherent counter-pumping.

It is shown in Figure 5.5 (b) that the pumping efficiency for DisFRAs with incoherent co-pumping is increased compared to incoherent counter-pumping. To achieve the same average gain, the pumping power of incoherent co-pumping is 50 mW less than that of incoherent counter-pumping.

In conclusion, simulation results show that C-band DisFRAs with incoherent co-pumping are superior to incoherent counter-pumping since the NF and OSNR flatness are improved, NF is reduced, OSNR is increased, and pumping power is also decreased.

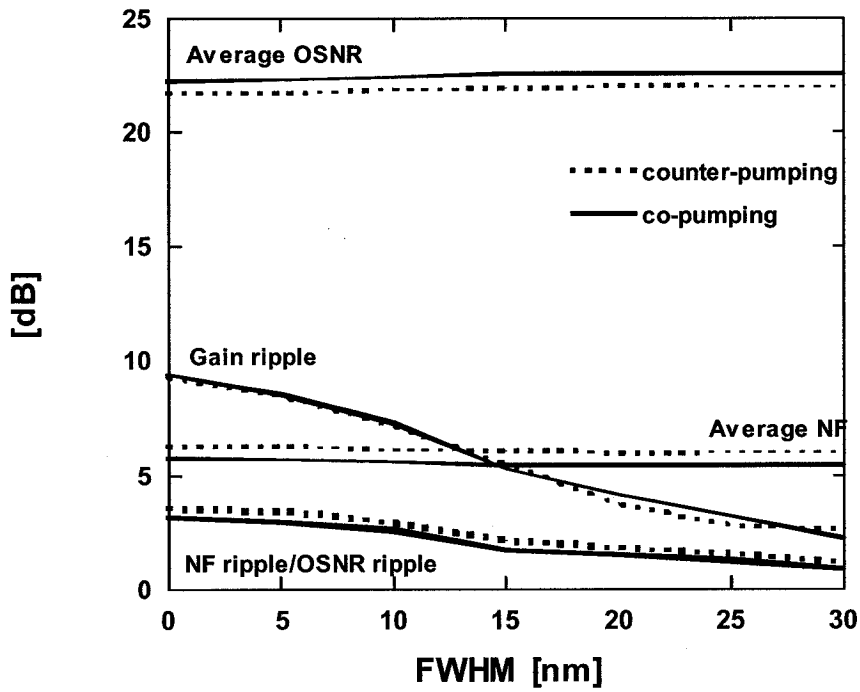

(a)

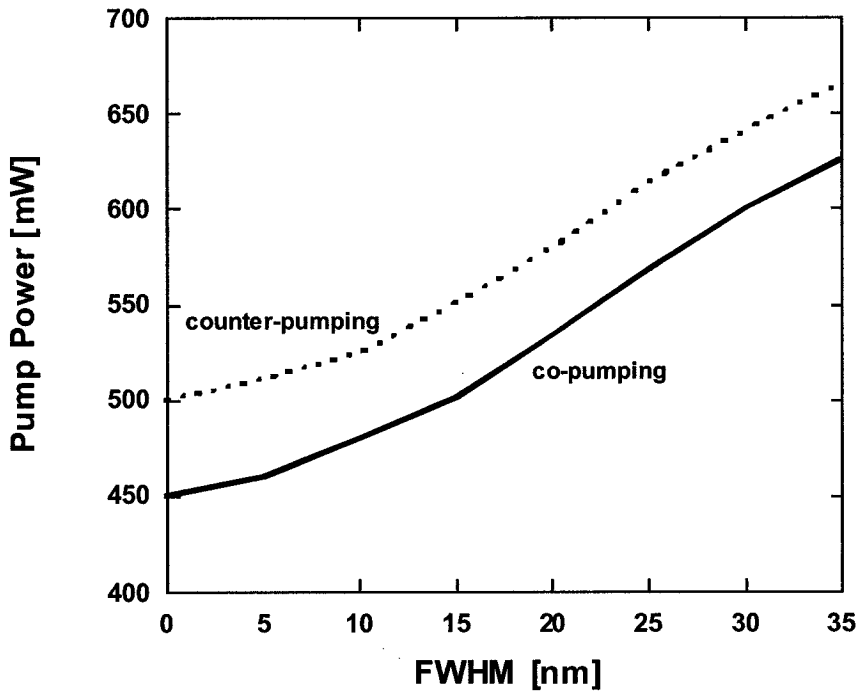

(b)

Figure 5.5 - The performance of C-band DisFRAs with one incoherent counter- or co-pumping source. (a) Gain ripple, average NF, NF ripple, average OSNR, and OSNR ripple and (b) Pumping power.

Table 5.5 Detailed simulation results for C-band DisFRAs with one incoherent pumping source

One incoherent co- or counter-pumping source								
FWHM [nm]	Pumping direction	C.W. [nm]	Power [mW]	Gain ripple [dB]	Average NF [dB]	NF ripple [dB]	Average OSNR [dB]	OSNR ripple [dB]
0	Co	1455	450	9.4	5.7	3.1	22.2	3.2
	Counter		500	9.3	6.3	3.5	21.7	3.6
5	Co	1454	460	8.5	5.7	2.9	22.3	3.0
	Counter		511	8.5	6.3	3.3	21.7	3.5
10	Co	1451	480	7.3	5.6	2.5	22.4	2.6
	Counter		525	7.1	6.1	2.8	21.9	2.9
15	Co	1450	501	5.2	5.4	1.8	22.6	1.8
	Counter		551	5.5	6.0	2.1	22.0	2.1
20	Co	1445	534	4.1	5.4	1.4	22.6	1.5
	Counter		580	3.7	6.0	1.7	22.0	1.8
25	Co	1440	568	3.2	5.4	1.2	22.5	1.3
	Counter		614	2.8	6.0	1.5	22.0	1.6
30	Co	1435	600	2.3	5.5	0.9	22.5	1.0
	Counter		641	2.6	6.0	1.2	22.0	1.2
35	Co	1425	626	2.3	5.5	0.8	22.4	0.9
	Counter		666	1.9	6.0	1.1	22.0	1.1

CHAPTER 6 PERFORMANCE COMPARISON OF L-BAND DISFRAs WITH INCOHERENT PUMPING TO COHERENT PUMPING

In this chapter, the performance of L-band DisFRAs with incoherent pumping is investigated and compared to conventional coherent pumping. All comparisons in this chapter are based on the same parameters: a fiber length of 8 km with the fiber type of OFS-DCF, 40 signal channels with channel spacing of 120 GHz over the spectrum of from 1570 to 1610 nm, -20 dBm per channel for input power and the average gain of 20 dB. In our analysis, we always optimize the pumping wavelengths of pumping sources for L-band DisFRAs to realize the gain as flat as possible.

L-band DisFRAs with counter-pumping are analyzed in Section 6.1. Our investigation explores the relationship of gain ripple, average NF, NF ripple, average OSNR, OSNR ripple, and pumping efficiency with FWHM of an incoherent counter-pumping source and compares the performance of L-band DisFRAs with multiple coherent counter-pumping sources to multiple incoherent counter-pumping sources. The above investigation is also carried out in Section 6.2, however, the L-band DisFRAs are co-pumped. The performance of L-band DisFRAs with incoherent co-pumping is compared to incoherent counter-pumping in Section 6.3. Simulation results show that L-band DisFRAs with incoherent co-pumping are preferred due to flatter NF and OSNR, lower NF, higher OSNR, and increased pumping efficiency.

6.1 L-band DisFRAs with counter-pumping

This section focuses on L-band DisFRAs with counter-pumping. We first consider one counter-pumping source [30]. We optimize an incoherent counter-pumping source with a FWHM of 15 nm and 30 nm to realize the flattest gain and the optimal center wavelengths are 1485 nm and 1471 nm, respectively. The coherent pumping can be considered as a special case of incoherent pumping, i.e., FWHM=0. The simulation results are listed in Table 6.1. Gain, NF, and OSNR are shown in Figure 6.1.

The gain ripple is 8.4, 5.0 and 2.2 dB, the average NF is 6.0, 5.8 and 5.7 dB, the NF ripple is 2.4, 1.6 and 0.9 dB, the average OSNR is 22.1, 22.3 and 22.5 dB, and the OSNR ripple is 2.4, 1.7, and 1.0 dB for DisFRAs with one coherent pumping source and one incoherent pumping source with a FWHM of 15 and 30 nm, respectively. The gain flatness is improved with the increase of FWHM of the incoherent pumping source. Apparently, the average NF and OSNR for DisFRAs with incoherent pumping are similar to coherent pumping because of the same average gain. Both the NF flatness and the OSNR flatness are improved with the increase of FWHM of the incoherent pumping source.

The pumping power is 510, 559 and 650 mW for DisFRAs with one coherent pumping source and one incoherent pumping source with a FWHM of 15 and 30 nm, respectively. Pumping efficiency is decreased with the increase of FWHM of the incoherent pumping source due to the fact that a larger portion of incoherent pumping power contributes to the Raman amplification for the spectrum of outside the L-band (i.e.

ASE noise).

Table 6.1 Detailed simulation results for L-band DisFRAs with one counter-pumping source

One coherent or incoherent counter-pumping source						
Pump	1^{th} Incoherent pump		2^{th} Incoherent pump		Coherent pump	
	Power [mW]	559	Power [mW]	650	Power [mW]	510
	C.W. [nm]	1485	C.W. [nm]	1471	C.W. [nm]	1490
	FWHM [nm]	15	FWHM [nm]	30	FWHM [nm]	0
Gain ripple [dB]	5.0		2.2		8.4	
Average NF [dB]	5.8		5.7		6.0	
NF ripple [dB]	1.6		0.9		2.4	
Average OSNR [dB]	22.3		22.5		22.1	
OSNR ripple [dB]	1.7		1.0		2.4	

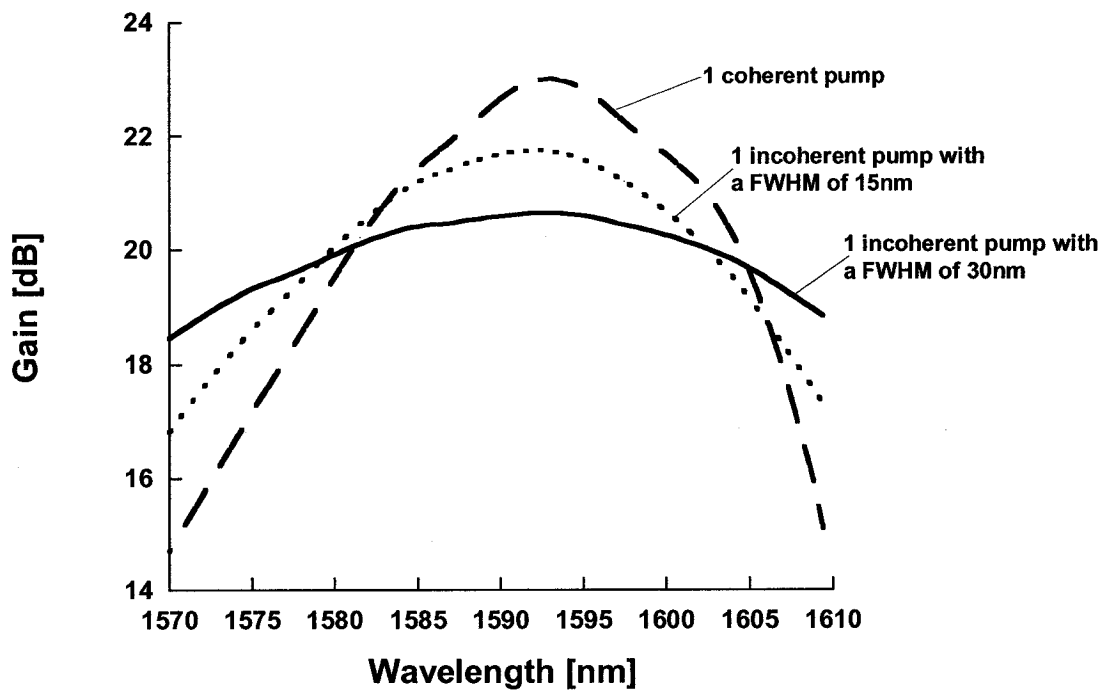

(a)

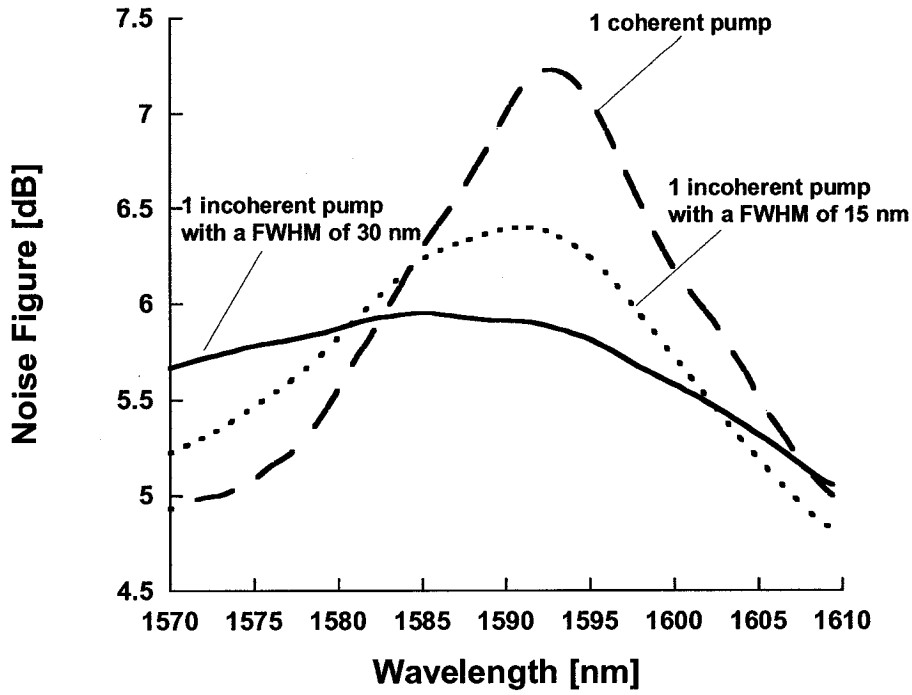

(b)

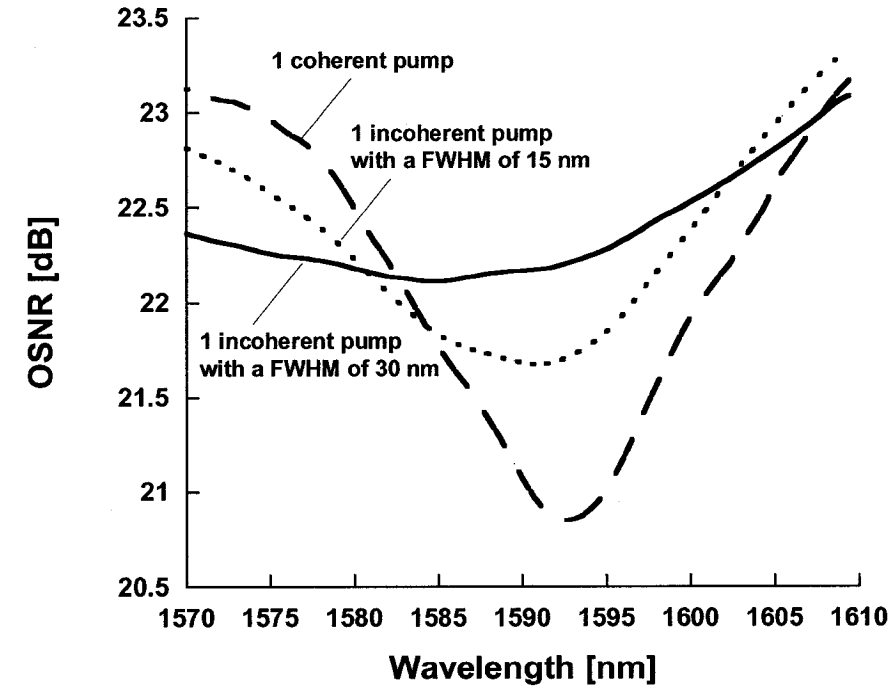

(c)

Figure 6.1 - The performance of L-band DisFRAs with one coherent counter-pumping source or one incoherent counter-pumping source with a FWHM of 15

or 30 nm. (a) Gain, (b) NF, and (c) OSNR

In the above analysis, only one pumping source was used for DisFRAs. We extend our study using multiple counter-pumping sources in the following. We consider L-band DisFRAs with two incoherent counter-pumping sources [30]. By optimization of two incoherent pumping wavelengths to obtain the flattest gain, it is found that the incoherent pumping sources should have a center wavelength at 1462 nm and the other wavelength at 1504 nm, both with a FWHM of 15 nm. For comparison, we also optimized DisFRAs with two or four coherent pumping sources. The simulation results are listed in Table 6.2 and Figure 6.2 shows the gain, NF, and forward noise power for the DisFRAs with coherent or incoherent pumping.

The gain ripple is 1.6, 0.7 and 0.3 dB, the average NF is 5.6, 5.7 and 5.7 dB, the NF ripple is 0.9, 0.9 and 0.9 dB, the average OSNR is 22.5, 22.4 and 22.4 dB, and the OSNR ripple is 1.0, 1.0, and 1.0 dB for DisFRAs with two, four coherent pumping sources and two incoherent pumping sources, respectively. L-band DisFRAs with two incoherent pumping sources have significantly flatter gain. Apparently, the average NF and OSNR for DisFRAs with incoherent pumping are similar to coherent pumping. Both the NF flatness and the OSNR flatness by using incoherent pumping are similar to coherent pumping. As seen in Figure 6.2 (b), the NF by using incoherent pumping is slightly degraded at the shorter wavelengths (1570-1585 nm). To understand that behavior, calculated forward noise spectra for the above three cases are illustrated in Figure 6.2 (c). The higher forward noise power at shorter wavelengths contributes to the NF increase. As

we have mentioned in Section 2.2, MPI and single-pass reflected noise degrades the noise performance. The noise degradation increases with gain due to MPI. Almost all the single-pass reflected noise has the larger gain at the amplifier output end for DisFRAs with counter-pumping compared to co-pumping [1].

The pumping power is 590, 638 and 694 mW for DisFRAs with two, or four coherent pumping sources or two incoherent pumping sources. Pumping efficiency is decreased for DisFRAs with incoherent pumping due to the fact that a larger portion of incoherent pumping power contributes to the Raman amplification for the spectrum of outside the L-band (i.e. ASE noise).

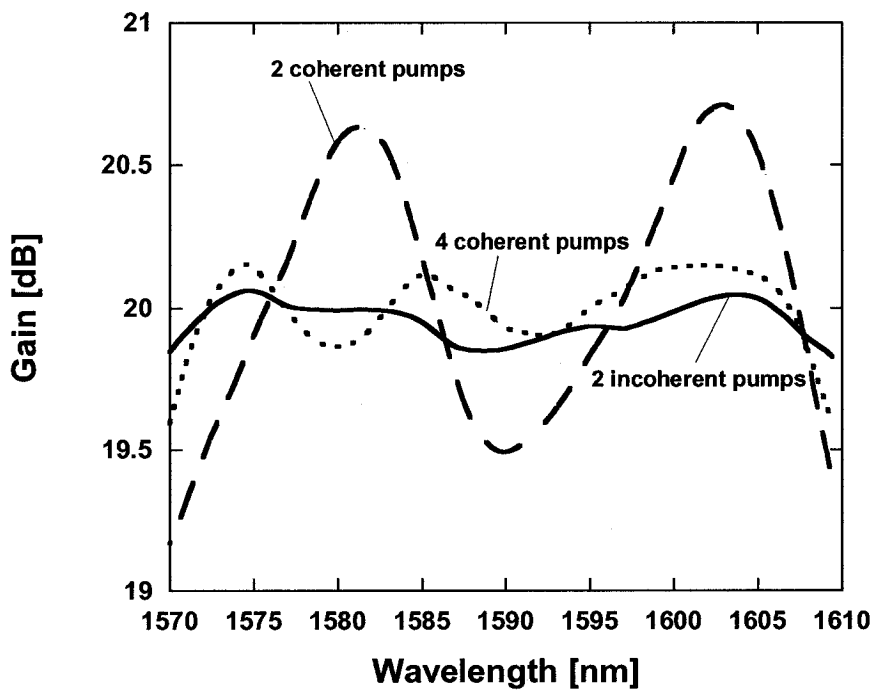

(a)

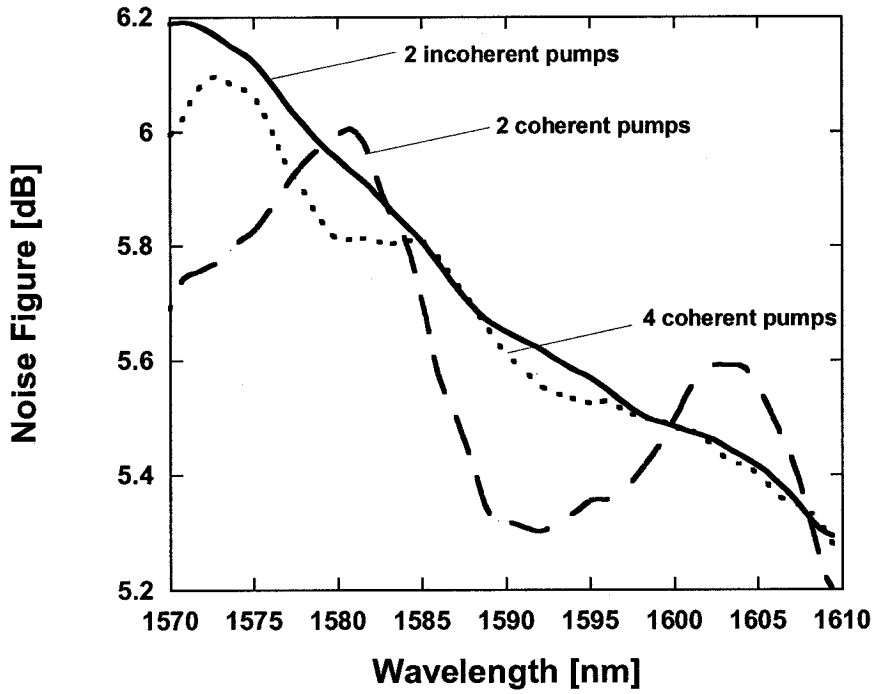

(b)

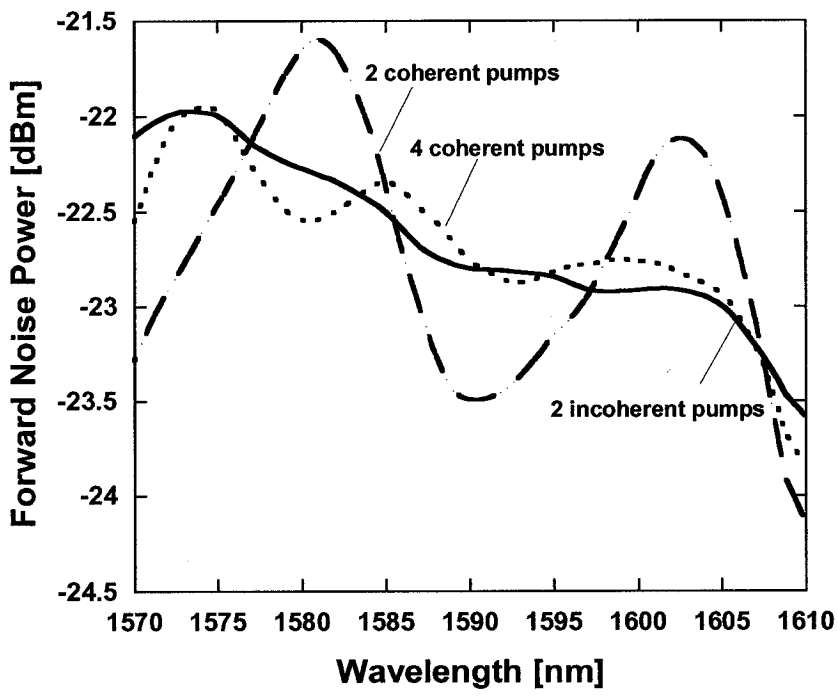

(c)

Figure 6.2 - (a) Gain, (b) NF, and (c) Forward noise power for L-band DisFRAs with two, or four coherent counter-pumping sources or two incoherent counter-pumping sources

Table 6.2 Detailed simulation results for L-band DisFRAs with multiple counter-pumping sources

Multiple coherent or incoherent counter-pumping sources											
Pump	2 Incoherent pumps			2 Coherent pumps			4 Coherent pumps				
	Total power [mW]		694	Total power [mW]		590	Total power [mW]		638		
	1	FWHM [nm]	15	1	Power [mW]	378	1	Power [mW]	257		
		C.W. [nm]	1462		C.W. [nm]	1469		C.W. [nm]	1462		
	2	FWHM [nm]	15	2	Power [mW]	212	2	Power [mW]	166		
		C.W. [nm]	1504		C.W. [nm]	1499		C.W. [nm]	1473		
							3	Power [mW]	147		
								C.W. [nm]	1493		
							4	Power [mW]	68		
								C.W. [nm]	1513		
Gain ripple [dB]	0.3			1.6			0.7				
Average NF [dB]	5.7			5.6			5.7				
NF ripple [dB]	0.9			0.9			0.9				
Average OSNR [dB]	22.4			22.5			22.4				
OSNR ripple [dB]	1.0			1.0			1.0				

6.2 L-band DisFRAs with co-pumping

In this section, we discuss L-band DisFRAs with co-pumping. We first consider L-band DisFRAs with one co-pumping source [30]. For the coherent pumping, it was

found that the pumping wavelength at 1490 nm provides the flattest gain over the L-band. For incoherent pumping with a FWHM of 15 and 30 nm, our optimization to achieve the flattest gain showed that the optimal pumping wavelengths are 1485 and 1471 nm for the pumping source having FWHM of 15 and 30 nm, respectively. Gain, NF, and OSNR are shown separately in Figure 6.3 for DisFRAs with coherent or incoherent pumping. Simulation results are listed in Table 6.3.

The gain ripple is 8.5, 4.8, and 2.2 dB, the average NF is 5.5, 5.3, and 5.3 dB, the NF ripple is 2.2, 1.4, and 0.7 dB, the average OSNR is 22.5, 22.8, and 22.8 dB, and OSNR ripple is 2.2, 1.4, and 0.8 dB for DisFRAs with coherent pumping and incoherent pumping with a FWHM of 15 nm and 30 nm, respectively. The gain flatness is improved with the increase of FWHM of the incoherent pumping source if we treat a coherent pump as a special case of an incoherent pump with FWHM=0. It is obvious that the average NF and OSNR for DisFRAs with incoherent pumping are similar to coherent pumping due to the same average gain. Both the NF flatness and the OSNR flatness are improved with the increase of FWHM of the incoherent pumping source.

The pumping power is 465, 516, and 612 mW for DisFRAs with coherent pumping and incoherent pumping with a FWHM of 15 nm and 30 nm, respectively. Pumping efficiency is decreased with the increase of FWHM of the incoherent pumping source due to the fact that a larger portion of incoherent pumping power contributes to the Raman amplification for the spectrum of outside the L-band (i.e. ASE noise).

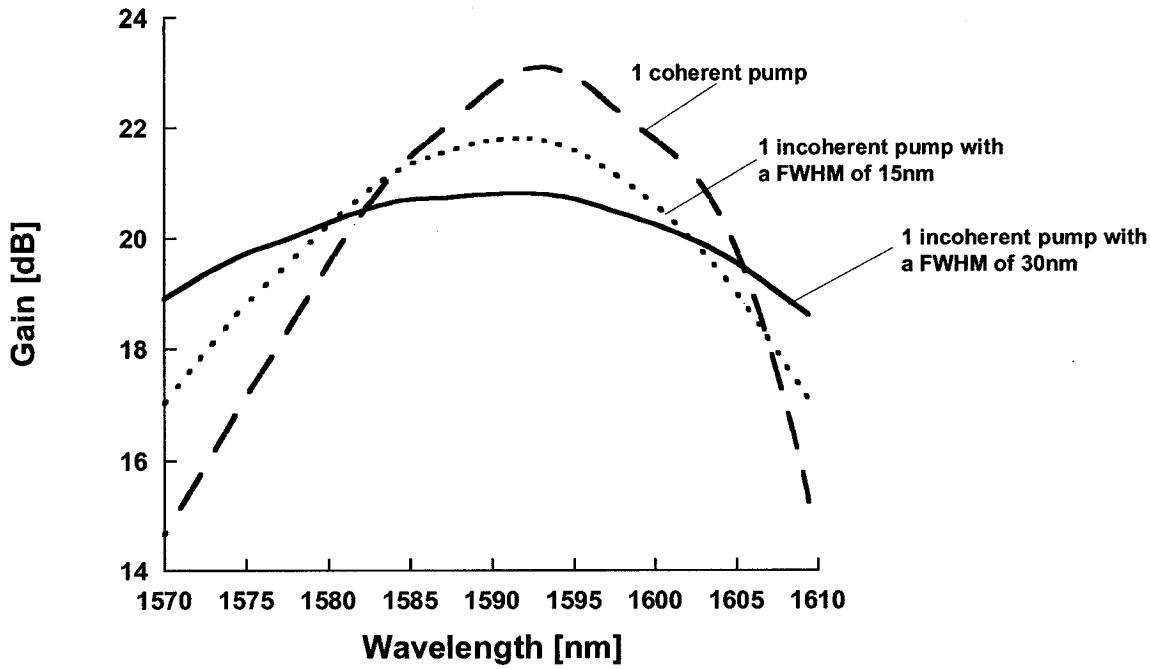
24
22
20
18
16
14
Gain [dB]
1 coherent pump
1 incoherent pump with
a FWHM of 15nm
1 incoherent pump with
a FWHM of 30nm
1570 1575 1580 1585 1590 1595 1600 1605 1610
Wavelength [nm]

(a)

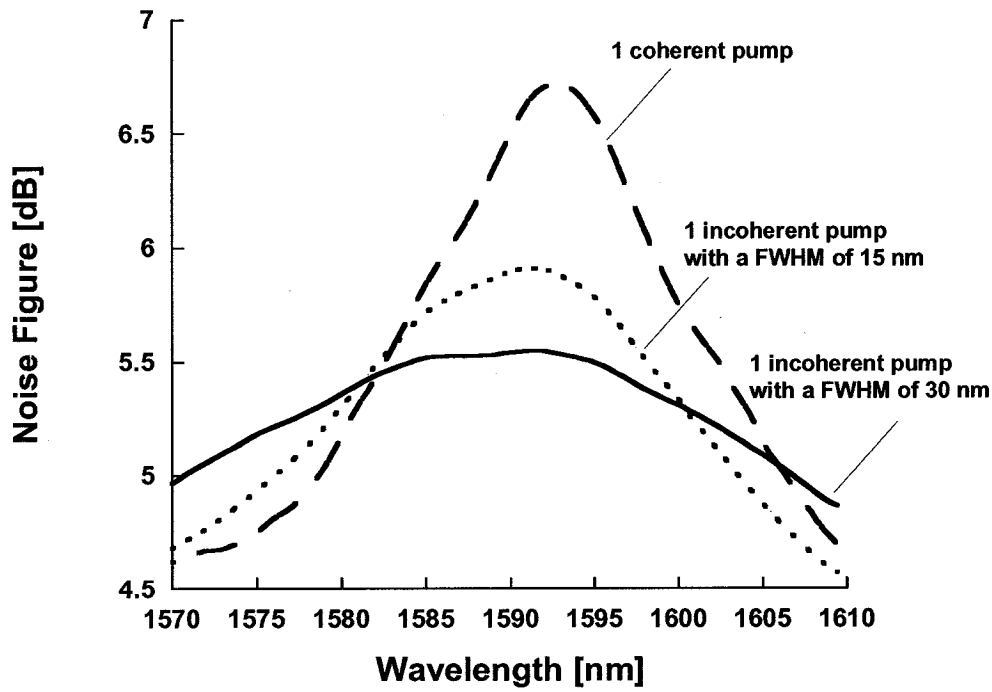
7
6.5
6
5.5
5
4.5
Noise Figure [dB]
1 coherent pump
1 incoherent pump
with a FWHM of 15 nm
1 incoherent pump
with a FWHM of 30 nm
1570 1575 1580 1585 1590 1595 1600 1605 1610
Wavelength [nm]

(b)

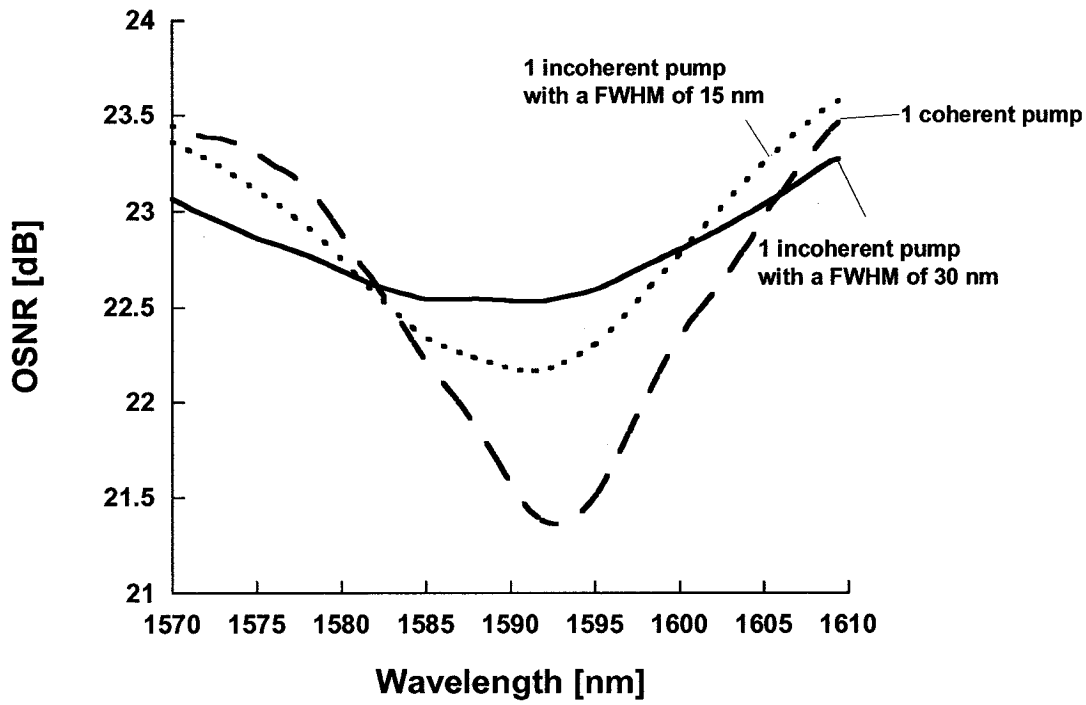

(c)

Figure 6.3 - (a) Gain, (b) NF, and (c) OSNR for L-band DisFRAs with one coherent co-pumping source and one incoherent co-pumping source with a FWHM of 15 and 30 nm, respectively

Table 6.3 Detailed simulation results for L-band DisFRAs with one co-pumping source

One coherent or incoherent co-pumping source						
Fiber	OFS DCF, 8 km					
Pump	1^{th} Incoherent pump		2^{th} Incoherent pump		Coherent pump	
	Power [mW]	516	Power [mW]	612	Power [mW]	465
	C.W. [nm]	1485	C.W. [nm]	1471	C.W. [nm]	1490
	FWHM [nm]	15	FWHM [nm]	30	FWHM [nm]	0
Gain ripple [dB]	4.8		2.2		8.5	
Average NF [dB]	5.3		5.3		5.5	
NF ripple [dB]	1.4		0.7		2.2	
Average OSNR [dB]	22.8		22.8		22.5	
OSNR ripple [dB]	1.4		0.8		2.2	

In the above analysis, only one pumping source was used for DisFRAs. We extend our study using multiple co-pumping sources in the following. By optimization of two incoherent co-pumping wavelengths to obtain the flattest gain, it is found that the incoherent pumping sources should have a center wavelength at 1462 nm and the other center wavelength at 1504 nm, both with a FWHM of 15 nm. For comparison, we also optimized DisFRAs with two or four coherent co-pumping sources. Figure 6.4 shows the gain, NF, and OSNR for DisFRAs with coherent or incoherent pumping. Simulation results are listed in Table 6.4.

The gain ripple is 1.5, 0.7 and 0.3 dB, the NF ripple is 0.6, 0.2, and 0.1 dB, the average NF is 5.2, 5.2, and 5.2 dB, the OSNR ripple is 0.6, 0.3, and 0.2 dB and the average OSNR is 22.9, 22.9 and 22.9 dB for the L-band DisFRAs with two, four coherent

pumping sources and two incoherent pumping sources, respectively. It is shown in Figure 6.4 (a) that DisFRAs with two incoherent pumping sources have significantly flatter gain compared to two or four coherent pumping sources. The average NF and OSNR for DisFRAs with incoherent pumping are similar to coherent pumping due to the same average gain. Both the NF flatness and the OSNR flatness are improved for DisFRAs with incoherent pumping compared to coherent pumping. As seen in Figure 6.4 (b), the NF spectrum resembles the gain spectrum in Figure 6.4 (a). As we have mentioned in Section 2.2, MPI and single-pass reflected noise degrades the noise performance. Because of MPI, the noise degradation increases with gain. Single-pass reflected noise has almost no impact on forward pumped amplifiers because most of the reflected noise does not have the high gain close to the fiber output end [1].

The pumping power is 549, 593 and 650 mW for DisFRAs with two, four coherent co-pumping sources and two incoherent co-pump sources, respectively. Pumping efficiency is decreased for DisFRAs with incoherent pumping due to the fact that a larger portion of pumping power contributes to the Raman amplification for the spectrum of outside the L-band (i.e. ASE noise).

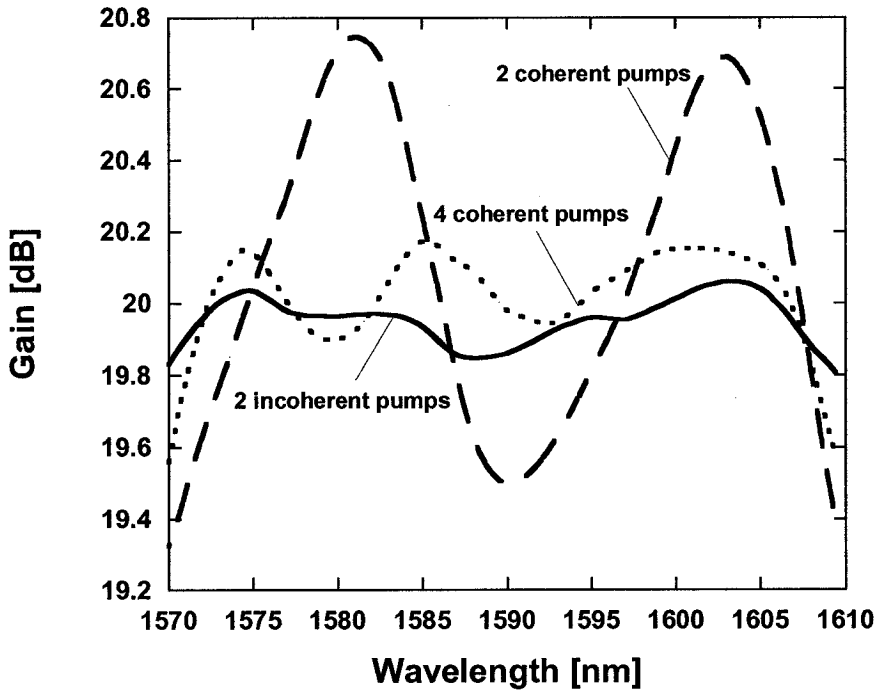
20.8
20.6
20.4
20.2
20
19.8
19.6
19.4
19.2
Gain [dB]
2 coherent pumps
4 coherent pumps
2 incoherent pumps
1570
1575
1580
1585
1590
1595
1600
1605
1610
Wavelength [nm]

(a)

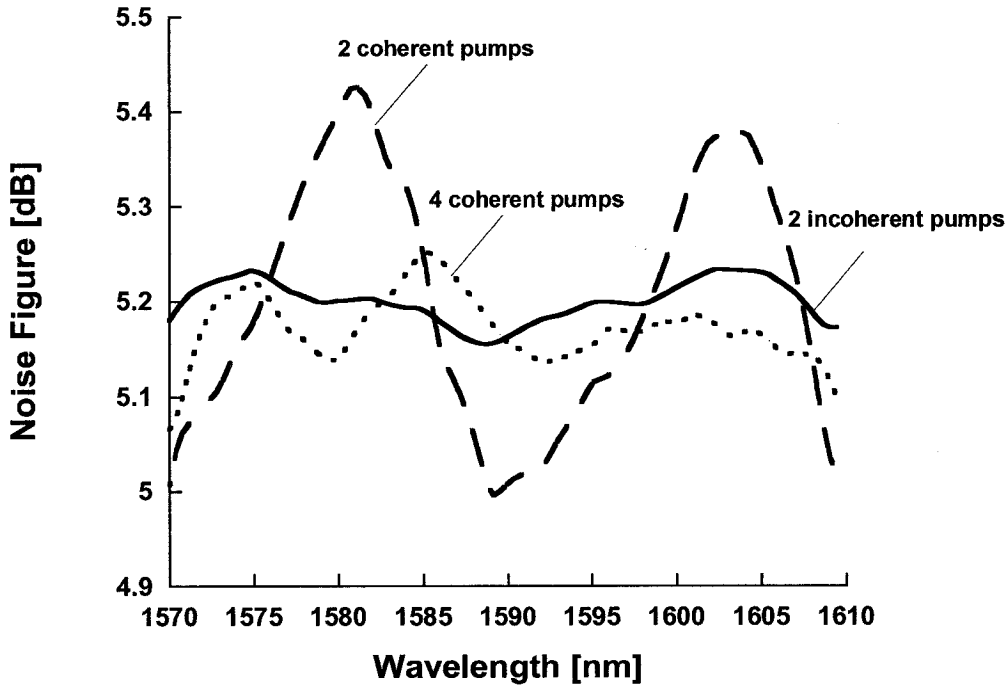
5.5
5.4
5.3
5.2
5.1
5
4.9
Noise Figure [dB]
2 coherent pumps
4 coherent pumps
2 incoherent pumps
1570
1575
1580
1585
1590
1595
1600
1605
1610
Wavelength [nm]

(b)

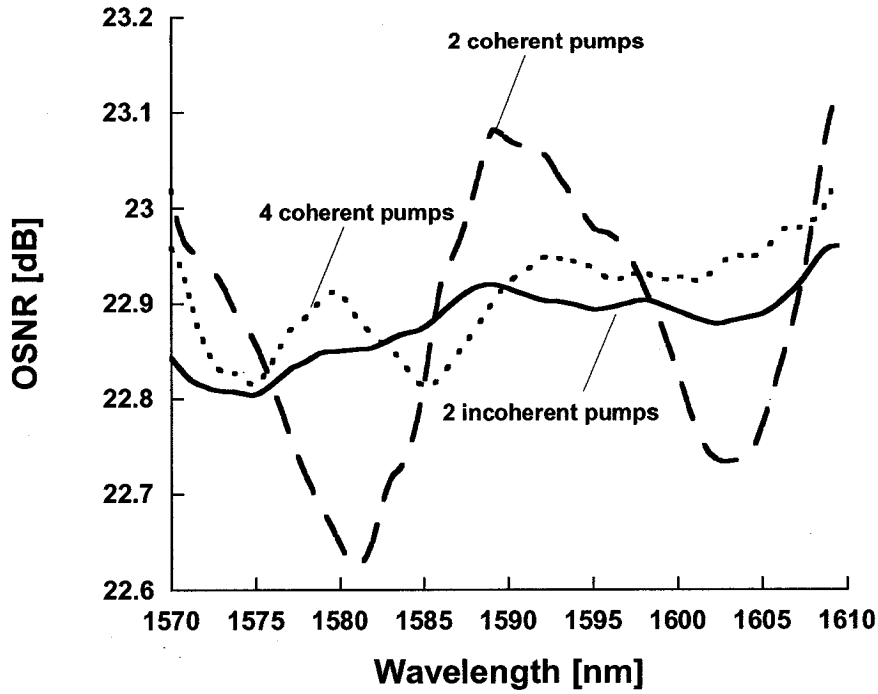

(c)

Figure 6.4 - (a) Gain, (b) NF, and (c) OSNR of L-band DisFRAs with two, or four coherent co-pumping sources or two incoherent co-pumping sources

Table 6.4 Detailed simulation results for L-band DisFRAs with multiple pumping sources

Multiple coherent or incoherent co-pumping sources											
Pump	2 Incoherent pumps			2 Coherent pumps			4 Coherent pumps				
	Total power [mW]		650	Total power [mW]		549	Total power [mW]		574		
	1	FWHM [nm]	15	1	Power [mW]	346	1	Power [mW]	224		
		C.W. [nm]	1462		C.W. [nm]	1469		C.W. [nm]	1428		
	2	FWHM [nm]	15	2	Power [mW]	203	2	Power [mW]	152		
		C.W. [nm]	1504		C.W. [nm]	1499		C.W. [nm]	1439		
							3	Power [mW]	141		
								C.W. [nm]	1459		
							4	Power [mW]	57		
								C.W. [nm]	1479		
Gain ripple [dB]	0.3			1.5			0.7				
Average NF [dB]	5.2			5.2			5.2				
NF ripple [dB]	0.1			0.6			0.2				
Average OSNR [dB]	22.9			22.9			22.9				
OSNR ripple [dB]	0.2			0.6			0.3				

6.3 The performance comparison of L-band DisFRAs with incoherent co-pumping to incoherent counter-pumping

This section focuses on the performance comparison of L-band DisFRAs with incoherent co-pumping to incoherent counter-pumping. The simulation results are listed

in Table 6.5. Figure 6.5 shows the gain, NF, and OSNR spectra for DisFRAs with one incoherent pumping source with a FWHM of 15 or 30 nm or two incoherent pumping sources with FWHM of 15 nm.

It is shown in Figure 6.5 (a) that the gain flatness for DisFRAs with co-pumping is similar to counter-pumping. The gain ripples obtained are 4.8/5.0, 2.2/2.2, and 0.3/0.3 dB for DisFRAs with one incoherent co-/counter-pumping source with a FWHM of 15 or 30 nm or two incoherent co-/counter-pumping sources with FWHM of 15 nm.

The average NF for DisFRAs with incoherent co-pumping is reduced around 0.47 dB compared to incoherent counter-pumping. The NF is degraded for DisFRAs with incoherent counter-pumping since almost all the single-pass reflected noise has the larger gain at the amplifier output end compared to incoherent co-pumping. Single-pass reflected noise has almost no impact on forward pumped amplifiers because most of the reflected noise does not have the high gain close to the fiber output end [1]. The average OSNR for DisFRAs with incoherent co-pumping is improved around 0.47 dB compared to incoherent counter-pumping.

The NF ripple is 1.4/1.6, 0.7/0.9, 0.1/0.9 dB and the OSNR ripple is 1.4/1.7, 0.8/1.0, 0.2/1.0 dB for DisFRAs with one incoherent co-/counter-pumping source with a FWHM of 15 or 30 nm or two incoherent co-/counter-pumping sources with FWHM of 15 nm. Both the NF flatness and the OSNR flatness by using co-pumping are improved compared to counter-pumping.

The pumping efficiency for DisFRAs with incoherent co-pumping is improved

compared to incoherent counter-pumping. To achieve the same average gain, the pumping power of incoherent co-pumping is about 40 mW less than that of incoherent counter-pumping.

In conclusion, simulation results show that L-band DisFRAs with incoherent co-pumping are preferred due to the flatter NF and OSNR, lower NF, higher OSNR, and increased pumping efficiency.

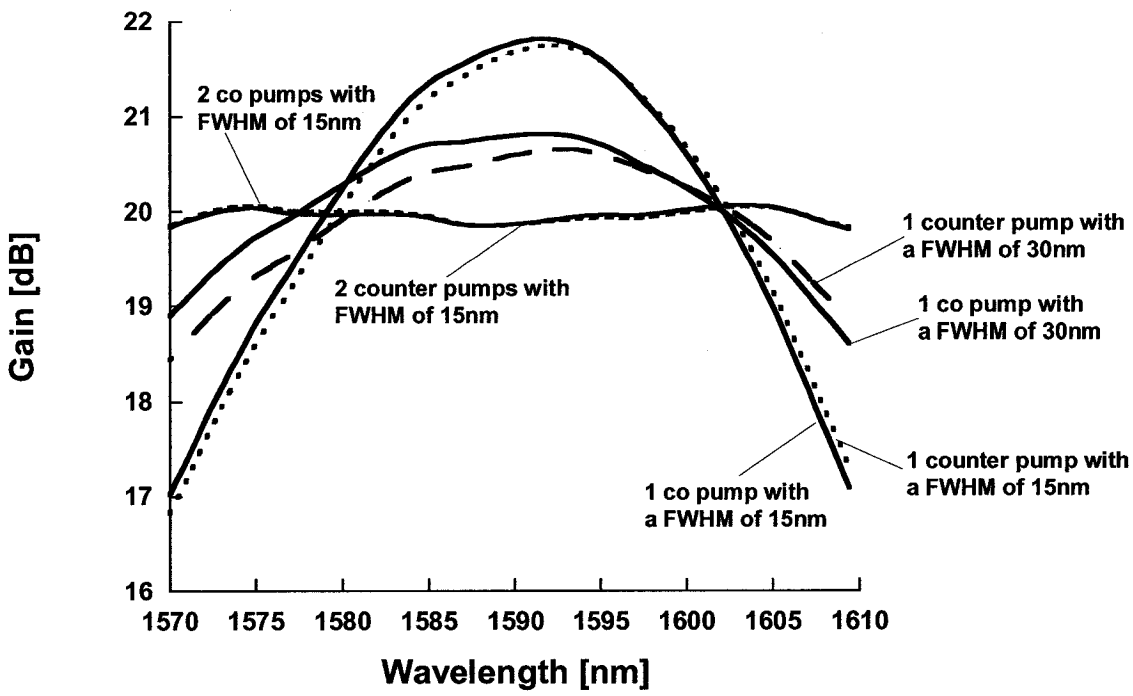

(a)

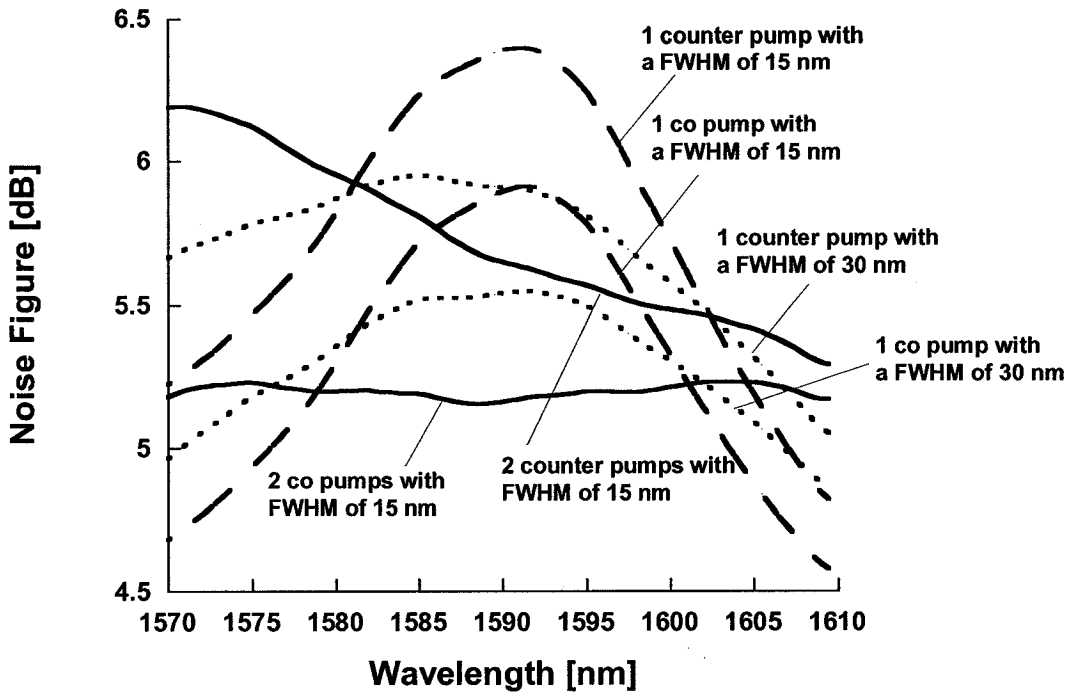

(b)

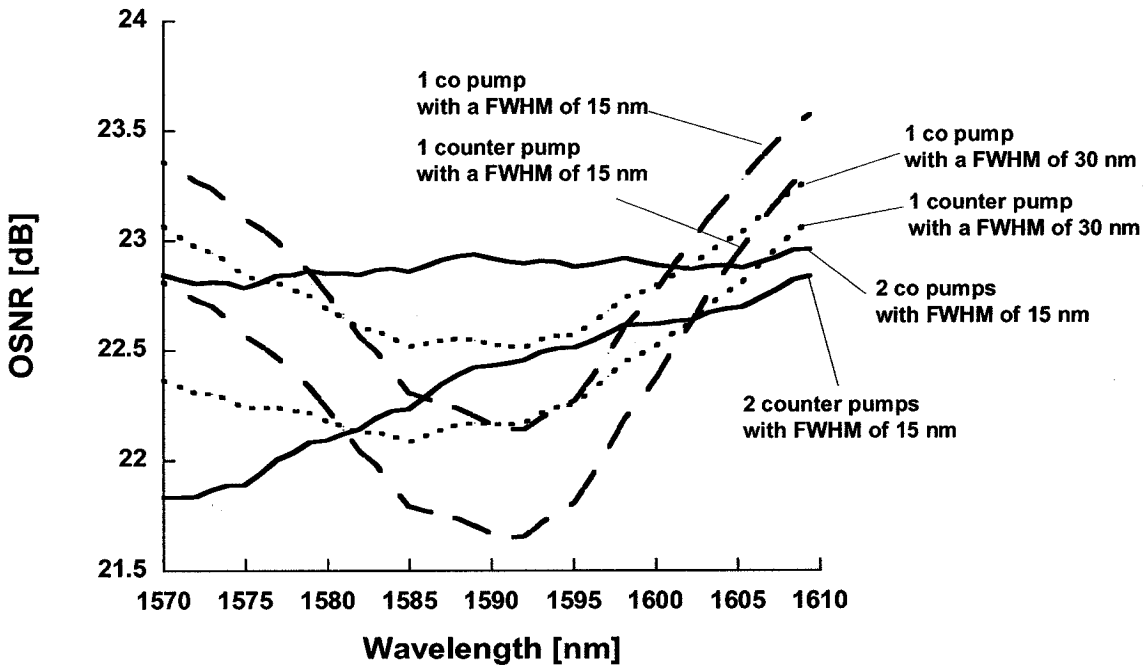

(c)

Figure 6.5 - The performance comparison for L-band DisFRAs with one or two incoherent co-/counter-pumping sources. (a) Gain, (b) NF, and (c) OSNR

Table 6.5 Detailed simulation results for L-band DisFRAs with incoherent pumping sources

One or two incoherent co-/ counter-pumping sources								
Pump Direction	Co	Counter	Co	Counter	Co		Counter-	
FWHM [nm]	15	15	30	30	15	15	15	15
C.W. [nm]	1485	1485	1471	1471	1462	1504	1462	1504
Power [mW]	516	559	612	650	650		694	
Gain ripple [dB]	4.8	5.0	2.2	2.2	0.3		0.3	
Average NF [dB]	5.3	5.8	5.3	5.7	5.2		5.7	
NF ripple [dB]	1.4	1.6	0.7	0.9	0.1		0.9	
Average OSNR [dB]	22.8	22.3	22.8	22.4	22.9		22.4	
OSNR ripple [dB]	1.4	1.7	0.8	1.0	0.2		1.0	

CHAPTER 7 PERFORMANCE COMPARISON OF C+L-BAND DISFRAs WITH INCOHERENT PUMPING TO COHERENT PUMPING

The performance comparisons of C-band and L-band DisFRAs with incoherent pumping to coherent pumping are presented in above two chapters, respectively. We continue our comparison for C+L-band DisFRAs in this chapter. All comparisons in this chapter are based on the same parameters: a fiber length of 8 km with the fiber type of OFS-DCF, 184 signal channels with channel spacing of 50 GHz over the spectrum of from 1530 to 1605 nm, -20 dBm per channel for input power and the average gain of 15 dB. In our analysis, we always optimize the pumping wavelengths of pumping sources for C+L-band DisFRAs to realize the gain as flat as possible.

. We compare the C+L-band DisFRAs with two incoherent counter-pumping sources to two, or four, or six coherent counter-pumping sources in terms of gain ripple, average NF, NF ripple, average OSNR, OSNR ripple and pumping efficiency in Section 7.1. We also compare the performance of C+L-band DisFRAs with two incoherent co-pumping sources to multiple coherent co-pumping sources in Section 7.2. The performance of C+L-band DisFRAs with incoherent co-pumping is compared to incoherent counter-pumping in Section 7.3. Simulation results show that C+L-band DisFRAs with incoherent co-pumping perform better because of flatter NF and OSNR, lower NF, higher OSNR, and increased pumping efficiency.

7.1 C+L-band DisFRAs with counter-pumping

This section focuses on C+L-band DisFRAs with counter-pumping. By optimization of two incoherent counter-pumping wavelengths to obtain the flattest gain, it is found that the incoherent pumping sources should have a center wavelength at 1423 nm and the other wavelength at 1494 nm, both with a FWHM of 30 nm. For comparison, we also optimized DisFRAs with two, or four, or six coherent counter-pumping sources. The simulation results are listed in Table 7.1 for DisFRAs with coherent pumping and in Table 7.2 for DisFRAs with incoherent pumping. Figure 7.1 shows the gain, NF, and forward noise power for DisFRAs with coherent or incoherent pumping.

The gain ripple is 4.1, 1.0, 0.7 and 0.6 dB, the average NF is 5.2, 5.3, 5.5 and 5.4 dB, the NF ripple is 1.5, 1.8, 2.3, and 2.1 dB, the average OSNR is 26.8, 26.7, 26.5 and 26.6 dB, and the OSNR ripple is 1.7, 2.0, 2.5, and 2.3 dB for DisFRAs with two, four, six coherent counter-pumping sources and two incoherent counter-pumping sources, respectively. In the case of coherent pumping, the gain ripple decreased with the increase of pumping numbers [12][31]. The gain ripple for DisFRAs with two incoherent pumping sources is significantly reduced compared to two, or four, or six coherent pumping sources, which suggests that incoherent pumping provides a much flatter gain. Apparently, the average NF and OSNR for DisFRAs with incoherent pumping sources are similar to coherent pumping sources. The NF flatness and the OSNR flatness by using incoherent pumping are also similar to coherent pumping.

As seen in Figure 7.2 (b), the noise performance by using incoherent pumping is

slightly degraded at the shorter wavelengths (1530-1560 nm). To understand that behavior, calculated forward noise spectra for the above four cases are illustrated in Figure 7.2 (c). The higher forward noise power at shorter wavelengths contributes to the NF increase. As we have mentioned in Section 2.2, MPI and single-pass reflected noise degrades the noise performance of DisFRAs. The noise degradation increases with gain due to MPI. Almost all the single-pass reflected noise has the larger gain at the amplifier output end for DisFRAs with counter-pumping compared to co-pumping [1].

The pumping power is 556, 607, 640 and 670 mW for two, or four, or six coherent pumps and two incoherent pumps. Pumping efficiency is decreased for DisFRAs with incoherent pumping due to the fact that a larger portion of pumping power contributes to the Raman amplification for the spectrum of outside the C+L-band (i.e. ASE noise).

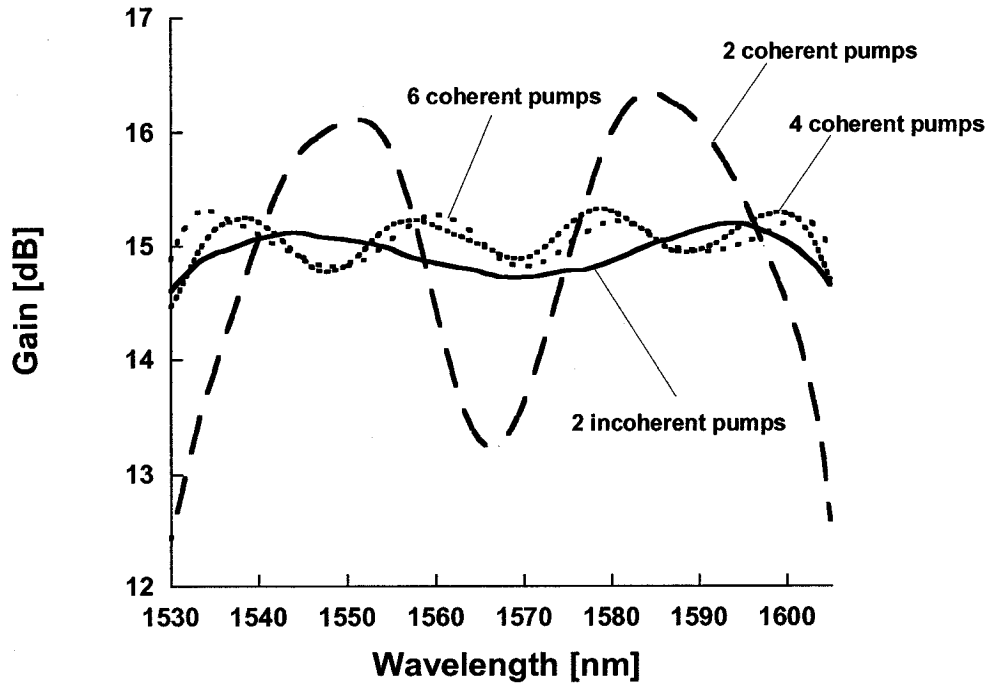

(a)

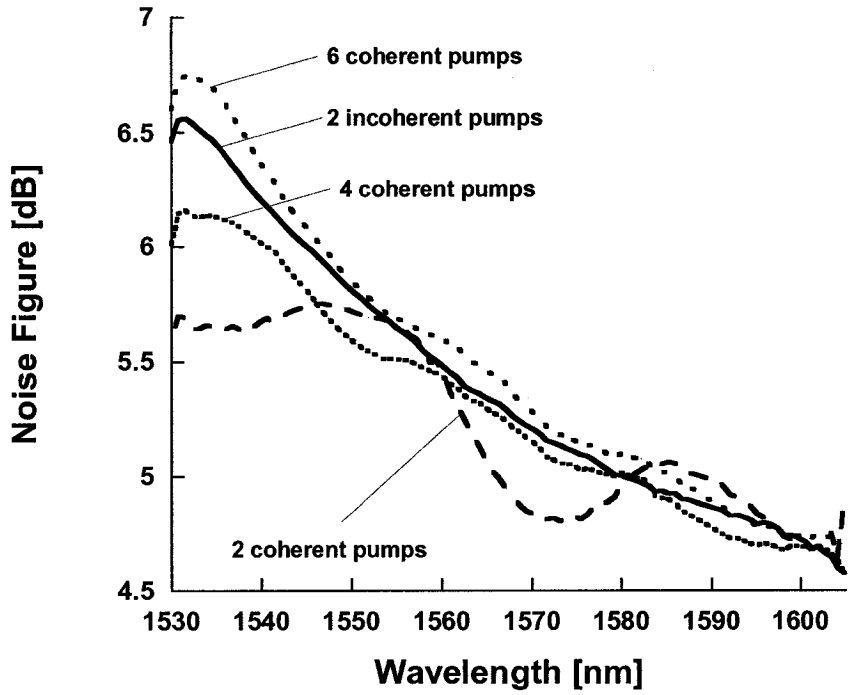

(b)

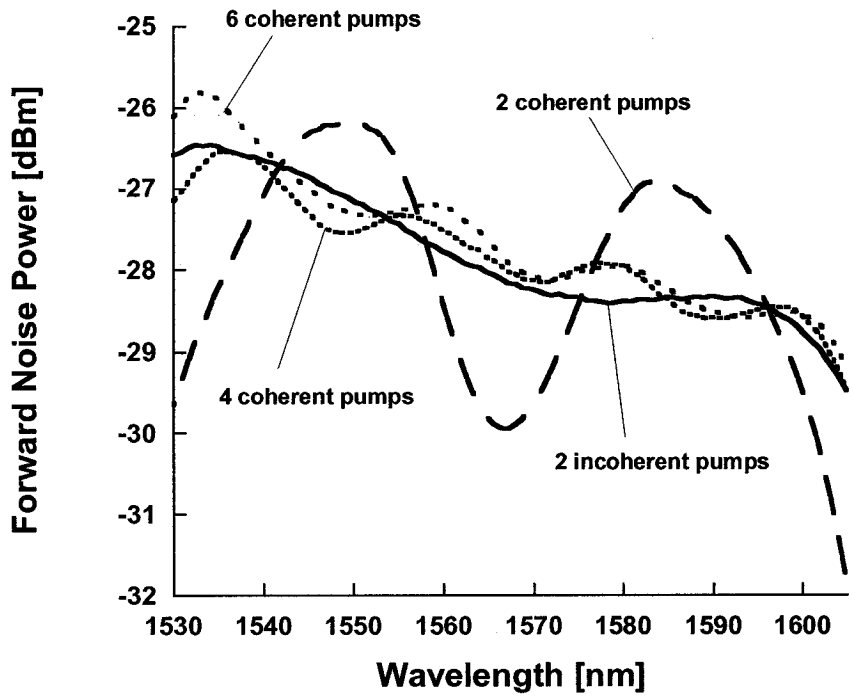

(c)

Figure 7.1 - (a) Gain, (b) NF, and (c) Forward noise spectra for C+L-band DisFRAs with

two, or four, or six coherent counter-pumping sources or two incoherent counter-pumping sources

Table 7.1 Detailed simulation results for C+L-band DisFRAs with two, or four, or six coherent counter-pumping sources

Two, or four, or six coherent counter-pumping sources									
	2 Coherent pumps			4 Coherent pumps			6 Coherent pumps		
	Total power [mW]		556	Total power [mW]		607	Total power [mW]		640
	1	Power [mW]	391	1	Power [mW]	284	1	Power [mW]	225
		C.W. [nm]	1447		C.W. [nm]	1432		C.W. [nm]	1428
	2	Power [mW]	165	2	Power [mW]	137	2	Power [mW]	150
		C.W. [nm]	1488		C.W. [nm]	1447		C.W. [nm]	1436
				3	Power [mW]	105	3	Power [mW]	110
					C.W. [nm]	1466		C.W. [nm]	1451
				4	Power [mW]	81	4	Power [mW]	75
					C.W. [nm]	1496		C.W. [nm]	1467
							5	Power [mW]	53
								C.W. [nm]	1487
							6	Power [mW]	27
								C.W. [nm]	1508
Gain ripple [dB]	4.1			1.0			0.7		
Average NF [dB]	5.2			5.3			5.5		
NF ripple [dB]	1.5			1.8			2.3		
Average OSNR [dB]	26.8			26.7			26.5		
OSNR ripple [dB]	1.7			2.0			2.5		

Table 7.2 Detailed simulation results for C+L-band DisFRAs with two incoherent counter-pumping sources

Two incoherent counter-pumping sources				
2 Incoherent Pumps	Power [mW]	670		
	C.W. [nm]	1423	C.W. [nm]	1494
	FWHM [nm]	30	FWHM [nm]	30
Gain ripple [dB]	Average NF [dB]	NF ripple [dB]	Average OSNR [dB]	OSNR ripple [dB]
0.6	5.4	2.1	26.6	2.3

7.2 C+L-band DisFRAs with co-pumping

In this section we consider C+L-band DisFRAs with co-pumping. The performance of C+L-band DisFRAs with multiple coherent pumping sources is compared to two incoherent pumping sources. By optimization of two incoherent pumping wavelengths to obtain the flattest gain, it is found that the incoherent pumping sources should have a center wavelength at 1423 nm and the other wavelength at 1494, both with a FWHM of 30 nm. For comparison, we also optimized DisFRAs with two, or four, or six coherent pumps. Figure 7.2 shows the gain, NF, and OSNR for DisFRAs with coherent or incoherent pumping. Simulation results are listed in Table 7.3 for DisFRAs with coherent pumping and in Table 7.4 for DisFRAs with incoherent pumping.

The gain ripples obtained are 3.1, 1.0, 0.7, and 0.6 dB, the average NF is 4.8, 4.8, 4.8 and 4.9 dB, the NF ripple is 1.2, 0.7, 0.7, and 0.5 dB, the average OSNR is 27.3, 27.3, 27.3, and 27.2 dB, and the OSNR ripple is 1.5, 0.9, 0.9, and 0.7 dB for DisFRAs with two, or four, or six coherent pumps or two incoherent pumps. It is shown in Figure 7.2 (a) that

DisFRAs with two incoherent pumping sources have significantly flatter gain compared to two, or four or six coherent pumping sources. The average NF and OSNR for DisFRAs with incoherent pumping are similar to coherent pumping due to the same average gain. Both the NF flatness and the OSNR flatness are improved for DisFRAs with incoherent pumping compared to coherent pumping. As seen in Figure 7.2 (b), the NF spectrum resembles the gain spectrum in Figure 7.2 (a). As we have mentioned in Section 2.2, MPI and single-pass reflected noise degrades the noise performance. Because of MPI, the noise degradation increases with gain. Single-pass reflected noise has almost no impact on forward pumped amplifiers because most of the reflected noise does not have the high gain close to the fiber output end [1].

The pumping power is 510, 554, 580 and 625 mW for DisFRAs with two, or four, or six coherent pumps or two incoherent pumps. Pumping efficiency is decreased for DisFRAs with incoherent pumping due to the fact that a larger portion of pumping power contributes to the Raman amplification for the spectrum of outside the C+L-band (i.e. ASE noise).

Table 7.3 Detailed simulation results for C+L-band DisFRAs with two, or four or six coherent co-pumping sources

Two, or four, or six coherent co-pumping sources												
	2 Coherent pumps			4 Coherent pumps			6 Coherent pumps					
	Total power [mW]		510	Total power [mW]		554	Total power [mW]		580			
	1	Power [mW]	355	1	Power [mW]	248	1	Power [mW]	183			
		C.W. [nm]	1447		C.W. [nm]	1432		C.W. [nm]	1428			
	2	Power [mW]	155	2	Power [mW]	130	2	Power [mW]	140			
		C.W. [nm]	1488		C.W. [nm]	1447		C.W. [nm]	1436			
				3	Power [mW]	95	3	Power [mW]	100			
					C.W. [nm]	1466		C.W. [nm]	1451			
				4	Power [mW]	81	4	Power [mW]	72			
					C.W. [nm]	1496		C.W. [nm]	1467			
							5	Power [mW]	54			
								C.W. [nm]	1487			
							6	Power [mW]	31			
								C.W. [nm]	1508			
Gain ripple [dB]	3.1			1.0			0.7					
Average NF [dB]	4.8			4.8			4.8					
NF ripple [dB]	1.2			0.7			0.7					
Average OSNR [dB]	27.3			27.3			27.2					
OSNR ripple [dB]	1.5			0.9			0.9					

Table 7.4 Detailed simulation results for C+L-DisFRAs with two incoherent co-pumping sources

Two incoherent co-pumping sources				
2 Incoherent Pumps	Power [mW]	625		
	C.W. [nm]	1423	C.W. [nm]	1494
	FWHM [nm]	30	FWHM [nm]	30
Gain ripple [dB]	Average NF [dB]	NF ripple [dB]	Average OSNR [dB]	OSNR ripple [dB]
0.6	4.9	0.5	27.2	0.7

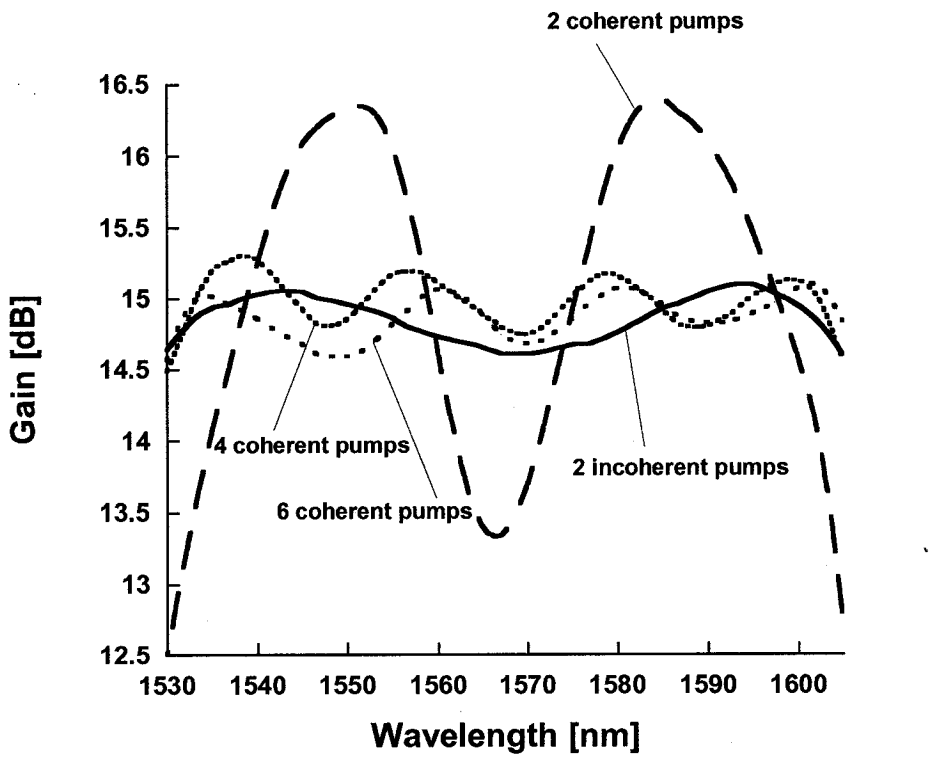

(a)

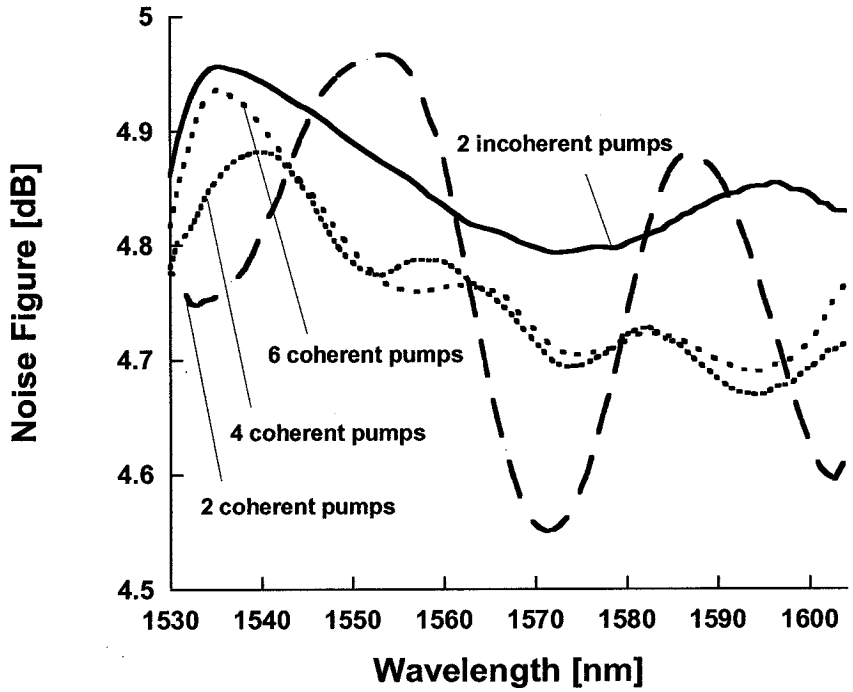
Noise Figure [dB]
5
4.9
4.8
4.7
4.6
4.5
2 incoherent pumps
6 coherent pumps
4 coherent pumps
2 coherent pumps
1530
1540
1550
1560
1570
1580
1590
1600
Wavelength [nm]

(b)

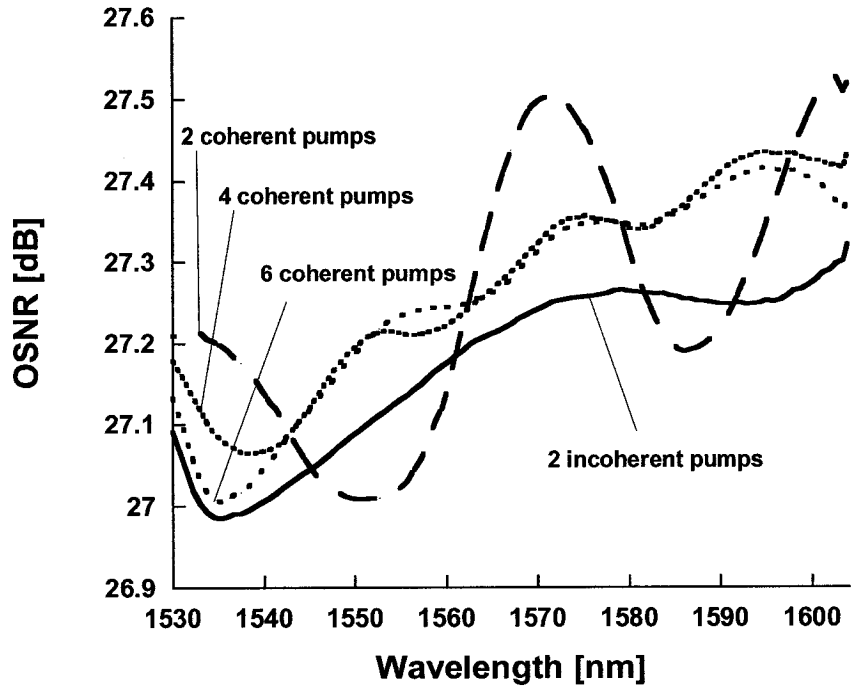
OSNR [dB]
27.6
27.5
27.4
27.3
27.2
27.1
27
26.9
2 coherent pumps
4 coherent pumps
6 coherent pumps
2 incoherent pumps
1530
1540
1550
1560
1570
1580
1590
1600
Wavelength [nm]

(c)

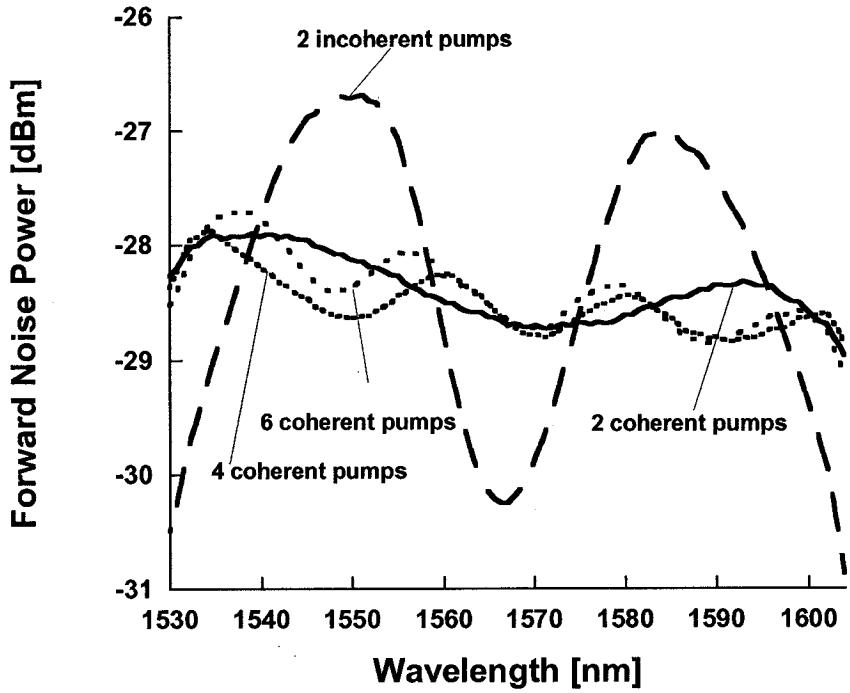

(d)

Figure 7.2 - Performance of C+L-band DisFRAs with coherent or incoherent pumping sources. (a) Gain, (b) NF, (c) OSNR, (d) Forward noise power

7.3 The performance comparison of C+L-band DisFRAs with incoherent co-pumping to incoherent counter-pumping

This section shows the performance comparison of C+L-band DisFRAs with incoherent co-pumping to incoherent counter-pumping. The simulation results are in Table 7.5. Figure 7.5 shows the gain, NF, and OSNR spectra for DisFRAs with two incoherent co-/counter-pumping sources with FWHM of 30 nm.

It is shown in Figure 7.5 (a) that DisFRAs with incoherent co-pumping sources have flatter gain compared to incoherent counter-pumping sources. The gain ripples obtained are 0.6/0.6 dB for DisFRAs with incoherent co-/counter-pumping. The average NF for

DisFRAs with incoherent co-pumping is improved 0.5 dB compared to incoherent counter-pumping. The NF is degraded for DisFRAs with incoherent counter-pumping since almost all the single-pass reflected noise has the larger gain at the amplifier output end compared to incoherent co-pumping. Single-pass reflected noise has almost no impact on forward pumped amplifiers because most of the reflected noise does not have the high gain close to the fiber output end [1]. The average OSNR for C+L-band DisFRAs with incoherent co-pumping is increased 0.4 dB compared to incoherent counter-pumping. To achieve the same average gain, the pumping power of incoherent co-pumping is 43 mW less compared to incoherent counter-pumping.

In conclusion, simulation results show that C+L-band DisFRAs with incoherent co-pumping are prior to incoherent counter-pumping because of the flatter NF and OSNR, lower NF, higher OSNR, and increased pumping efficiency.

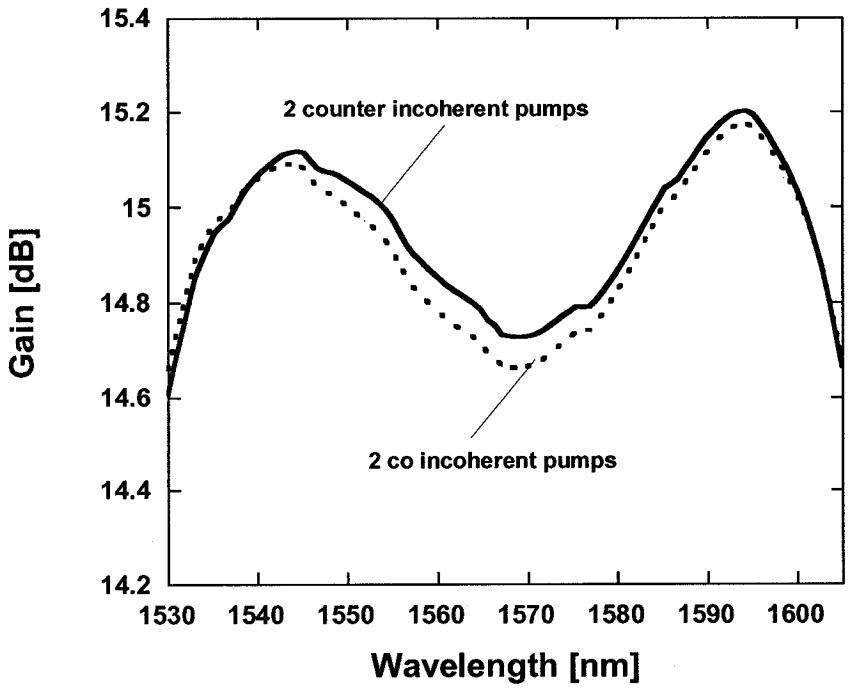

(a)

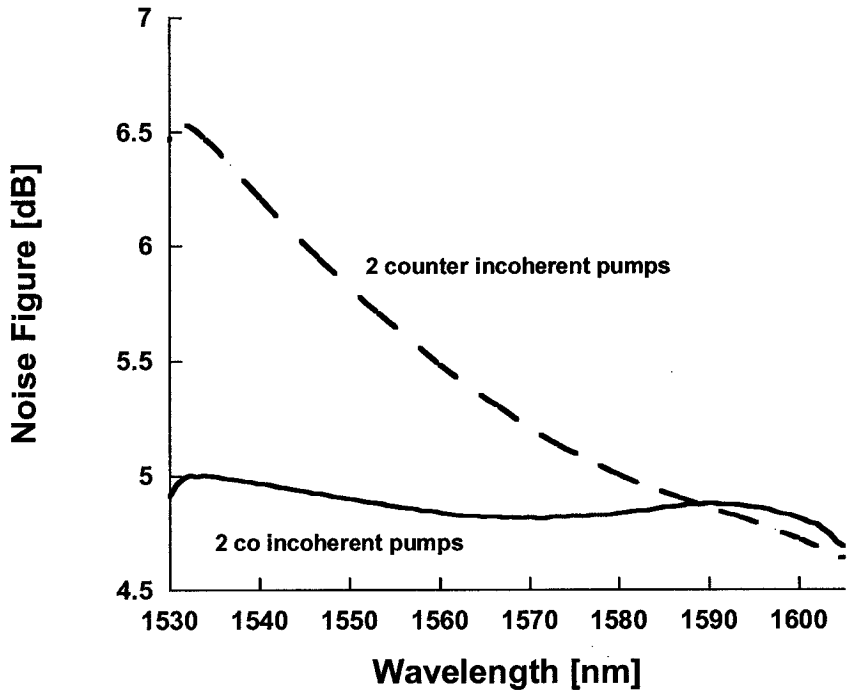

(b)

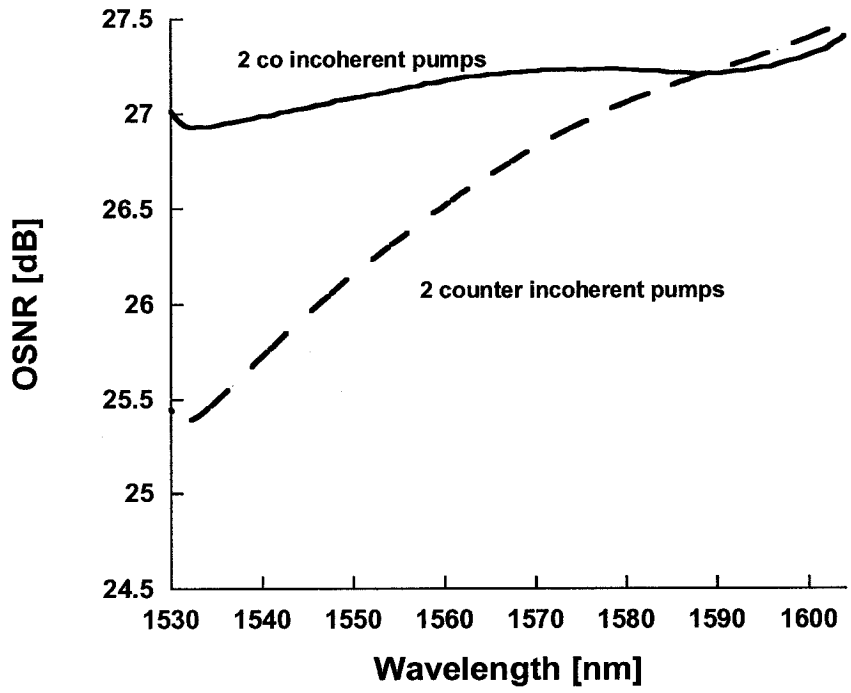

(c)

Figure 7.3 - The performance of C+L-band DisFRAs with two incoherent co-/counter-pumping sources. (a) Gain, (b) NF, (c) OSNR.

Table 7.5 Detailed simulation results for C+L-band DisFRAs with two incoherent co/counter-pumping sources

Two incoherent co/counter-pumping sources				
Pump Direction	Co		Counter-	
FWHM [nm]	30	30	30	30
C.W. [nm]	1423	1494	1423	1494
Power [mW]	627		670	
Gain ripple [dB]	0.6		0.6	
Average NF [dB]	4.9		5.4	
NF ripple [dB]	0.5		2.1	
Average OSNR [dB]	27.2		26.6	
OSNR ripple [dB]	0.7		2.3	

CHAPTER 8 CONCLUSIONS

In this thesis, C-band, L-band, and C+L-band DisFRAs with incoherent pumping are investigated respectively considering gain, NF, NF ripple, OSNR, OSNR ripple, and pumping efficiency with comparison to coherent pumping. All comparisons are based on the same average gain.

The performance comparison of C-band DisFRAs with incoherent pumping to coherent pumping is presented in Chapter 5. C-band DisFRAs with counter-pumping are analyzed in Section 5.1 and with co-pumping are analyzed in Section 5.2. Increasing the spectral bandwidth of the incoherent pumping source, gain ripple, NF ripple, and OSNR ripple decrease exponentially in dB and accordingly increase of pumping power exponentially in mW. To achieve the same gain flatness the number of pumps for C-band DisFRAs with incoherent pumping can be significantly reduced compared to coherent pumping. The performance of C-band DisFRAs with incoherent co-pumping is compared to incoherent counter-pumping in Section 5.3. The simulation results show that C-band DisFRAs with incoherent co-pumping are superior to incoherent counter-pumping due to flatter NF and OSNR, lower NF, higher OSNR and increased pumping efficiency.

The performance comparison of L-band DisFRAs with incoherent pumping to coherent pumping is given in Chapter 6. L-band DisFRAs with counter-pumping are investigated in Section 6.1 and with co-pumping are investigated in Section 6.2. The gain flatness, NF flatness, and OSNR flatness are improved and pumping efficiency is

decreased with the increase of FWHM of the incoherent pumping source. Apparently, the average NF and OSNR by using incoherent pumping are similar to coherent pumping due to the same average gain. To achieve the same gain flatness the number of pumps for L-band DisFRAs with incoherent pumping is reduced compared to coherent pumping. The performance of L-band DisFRAs with incoherent co-pumping is compared to incoherent counter-pumping in Section 6.3. Simulation results show that L-band DisFRAs with incoherent co-pumping perform better because of flatter NF and OSNR, lower NF, higher OSNR, and increased pumping efficiency.

We continue our comparison for C+L-band DisFRAs in Chapter 7. C+L-band DisFRAs with counter-pumping are analyzed in Section 7.1 and with co-pumping are analyzed in Section 7.2. We compare the C+L-band DisFRAs with two incoherent pumping sources to two, or four, or six coherent pumping sources. To achieve the same gain flatness the number of pumps for L-band DisFRAs with incoherent pumping is reduced compared to coherent pumping. The performance of C+L-band DisFRAs with incoherent co-pumping is also compared to incoherent counter-pumping in Section 7.3. Simulation results indicate that C+L-band DisFRAs with incoherent co-pumping are preferred because of flatter NF and OSNR, lower NF, higher OSNR, and increased pumping efficiency.

We believe that high-power incoherent pumping will expand the seamless gain bandwidth and could be employed in ultra-large-capacity DWDM systems employing the S-, C-, and L-bands.

References

[1] M. Nissov, "Long-Haul Optical Transmission Using Distributed Raman Amplification," *chapter 1, pp.2-13, December 1997, Ph.D. thesis.*

[2] J. Senior, "Optical Fiber Communications: Principles and Practice," *chapter 1, pp.1-11, Optoelectronics, Prentice Hall, New York, second edition, 1992.*

[3] F. Kapron, D. Keck, and R. Maurer, "Radiation Losses in Glass Optical Waveguides," *Applied Physics Letters, vol.17, pp.423-425, 1970.*

[4] T. Miya, Y. Terunuma, T. Hosaka, and T. Miyashita, "Ultimate Low-loss Single-mode Fiber at 1.55μm," *IEEE Electronics Letters, vol.15, pp.106, 1979.*

[5] R. Mears. L. Reekie, S. Poole, and D. Payne, "Low threshold tunable CW and Q-switched fiber user operating at 1.55μm," *IEEE Electronics Letters, vol.22, pp.159-160, 1986.*

[6] S. Poole, D. Payne, R. Mears, M. Fermann, and R. Laming, "Fabrication and characterization of low-loss optical fibers containing rare-earth ions," *Journal of Lightwave Technology, vol.4, pp.870-873, 1986.*

[7] A. Astakhov, M. Butusov, S. Galkin, N. Ermakova, and Y. Fedorov, "Fiber lasers with 1.54μm radiation wavelength". *Optical Spectrosc, vol.62, pp.140, 1987.*

[8] J. Bromage, "Raman Amplification for Fiber Communications Systems," *Journal of Lightwave Technology, vol.22, No.1, January 2004.*

[9] V. Perlin and H. Winful, "On Distributed Raman Amplification for Ultrabroad-Band Long-Haul WDM Systems," *Journal of Lightwave Technology, Vol.20, No.3, March 2002.*

[10] G.Agrawal, "Fiber-Optic Communication Systems: Evolution of Lightwave Systems," *Chapter 1, pp.62-63, The Institute of Optics University of Rochester, Rochester, NY, third edition, 2002.*

[11] M. Islam, "Raman amplifiers for telecommunications," *IEEE Journal of Quantum Electronics, vol. 8, pp.548–559, May/June 2002.*

[12] V. Perlin and H. Winful, "Optimal Design of Flat-Gain Wide-Band Fiber Raman Amplifiers," *Journal of Lightwave Technology, vol.20, No.2, February 2002.*

[13] T. Kung, C. Chang, J. Dung, and S. Chi, "Four-wave mixing between pump and signal in a distributed Raman amplifier, " *Journal of Lightwave Technology, vol. 21, pp.1164-1170, 2003.*

[14] J. Bouteiller, L. Leng, and C. Headley, "Pump-pump four-wave mixing in distributed Raman amplified systems," *Journal of Lightwave Technology, vol. 22, pp. 723-732, 2004.*

[15] G. Bolognini, S. Sugliani, and F. Pasquale, "Double Rayleigh scattering noise in Raman amplifiers using pump time-division-multiplexing schemes," *IEEE Photonics Technology Letters, vol. 16, pp. 1286-1288, 2004.*

[16] J. Bromage, P. Winzer, L. Nelson, M. Mermelstein, and C. Headley, "Amplified spontaneous emission in pulse-pumped Raman amplifiers," *IEEE Photonics Technology Letters, vol. 15, pp. 667-669, 2003.*

[17] J. Nicholson, J. Fini, J. Bouteiller, J. Bromage, and K. Brar, "Stretched ultrashort pulses for high repetition rate swept wavelength Raman pumping," *Journal of Lightwave Technology, vol.22, pp.71-78, 2004.*

[18] F. Pasquale and F. Meli, "New Raman pump module for reducing pump-signal four-wave-mixing interaction in co-pumped distributed Raman amplifiers," *Journal of Lightwave Technology, vol.22, pp. 1742-1748, 2003.*

[19] D. Yakhshoori, M. Azimi, P. Chn, B. Han, M. Jiang, K. Knopp, C. Lu, Y. Shen, G. Rhodes, S. Vote, P.D. Wang, X. Zhu, "Raman Amplification Using High-Power Incoherent Semiconductor Pump Sources," *PD47, OFC 2003.*

[20] John. Senior, "Optical Fiber Communications: Principles and Practice," *chapter 6, pp.243-251, Optoelectronics, second edition, 1992.*

[21] C. Raman and K. Krishnan, "A new type of secondary radiation," *Nature, vol.121, pp.501, 1928.*

[22] K. Rottwitt, J. Bromage, A. J.Stentz, L. Leng, M. Lines, and H. Smith, "Scaling of the Raman Gain Coefficient: Applications to Germanosilicate Fibers," *Journal of Lightwave Technology, vol.21, No.7, July 2003.*

[23] www.ahuracorp.com , *January 2005.*

[24] R. Essiambre, P. Winzer, J. Bromage, and C. Kim, "Design of Bi-directional Pumped Fiber Amplifiers Generating Double Rayleigh Backscattering," *IEEE Photonics Technology Letters, vol.14, No.7, July 2002.*

[25] R. Essiambre, P. Winzer, J. Bromage, and C. Kim, "Design of Bidirectionally Pumped Fiber Amplifiers Generating Double Rayleigh Backscattering," *IEEE Photonics Technology Letters, vol.14, No.7, July 2002.*

[26] I. Mandelbaum and M. Bolshtyansky, "Raman amplifier model in single-mode optical fiber," *IEEE Photonics Technology Letter, vol.15, pp.1704-1706, 2003.*

[27] H. Kidorf, K. Rottwitt, M. Nissov, M. Ma, and E. Rabarijaona, "Pump Interactions in a 100-nm Bandwidth Raman Amplifier," *IEEE Photonics Technology Letters, vol.11, No.5, May 1999.*

[28] X. Liu and B. Lee, "A fast and stable method for Raman amplifier propagation equations," *Optics Express, vol.11, No.18, 8 September 2003.*

[29] X. Liu and B. Lee "Effective shooting algorithm and its application to fiber amplifiers," *Optics Express, vol.11, No.12, 16 June 2003.*

[30] T. Zhang, X. Zhang and G. Zhang, "Distributed Fiber Raman Amplification with Incoherent Pumping, " *IEEE Photonics Technology letters, June 2005.*

[31] X. Liu, B. Lee, "Optimal design for ultra-broad band amplifiers," *Journal of Lightwave Technology, vol. 21, pp.3446-3455, 2003.*

Acronyms

ASE	amplified spontaneous emission
DCF	dispersion-compensating fiber
DFRA	distributed fiber Raman amplifier
DisFRA	discrete fiber Raman amplifier
DRB	double-Rayleigh backscattering
DWDM	dense wavelength division multiplexing
EDFA	erbium-doped fiber amplifier
FRA	fiber Raman amplifier
FWHM	full-width at half-maximum
FWM	four-wave-mixing
MPI	multiple-path interference
NF	noise figure
OSNR	optical signal to noise ratio
SBS	stimulated Brillouin scattering
SMF	standard silica fiber
SNR	signal-to-noise
SOA	semiconductor optical amplifier
SPOA	seeded power-optical-amplifier
SRS	stimulated Raman scattering
TDM	time-division multiplexed

XSE	excess spontaneous emission noise
WDM	wavelength division multiplexing